Energy Reports 8 (2022) 3189–3212

Contents lists available at ScienceDirect

Energy Reports

journal homepage: www.elsevier.com/locate/egyr

Research paper

Fresnel solar cooling plant for buildings: Optimal operation of an absorption chiller through inverse modelling

MCarmen Guerrero Delgado [a], Jose Sánchez Ramos [a], Daniel Castro Medina [a], Teresa Rocío Palomo Amores [a], Alberto Cerezo-Narváez [b,*], Servando Álvarez Domínguez [a]

[a] Grupo Termotecnia, Escuela Técnica Superior de Ingeniería, Universidad de Sevilla, Camino de los Descubrimientos S/N, 41092, Seville, Spain
[b] Departamento de Ingeniería Mecánica y Diseño Industrial, Escuela Superior de Ingeniería, Universidad de Cádiz, Avenida Universidad de Cádiz N° 10, 11519, Puerto Real, Cádiz, Spain

ARTICLE INFO

Article history:
Received 16 October 2021
Received in revised form 31 December 2021
Accepted 10 February 2022
Available online xxxx

Keywords:
Solar cooling plant
Absorption chiller
Double effect
Inverse modelling
Renewable energy integration

ABSTRACT

Increasing comfort conditions in buildings imply higher energy demands. However, these needs can be mitigated by solar cooling solutions. These systems, such as absorption chillers, are complex and require stable operation, with strict control to maximise the solar fraction and minimise gas consumption. This is incompatible with the variability of renewable resources, so they are often coupled with auxiliary gas systems. Although gas-free operation is possible if these systems are optimally controlled, they would require special supervision. This paper aims to develop an experimental validation of an inverse model to manage an absorption chiller coupled with a solar cooling plant. To know its real behaviour, long-term experiments have been performed using this plant, which consists of a linear Fresnel solar collector and an auxiliary natural gas boiler. The inverse model is used as a predictive control tool to decide the auxiliary boiler commands of the absorption chiller to optimise its operation: maximum cooling production by minimising gas consumption and maximising solar contribution. It has been identified with data from two weeks and validated with data from one summer month. Results show that the model estimates, on a time base of fewer than 30 min, are acceptable with errors of less than 5%. In addition, the maximum error of the estimated seasonal COP and the renewable fraction are less than 6% per day. Therefore, the results prove the usefulness of the proposal as a predictive control for optimal operation. Furthermore, it could be used as a baseline for preventive maintenance. If the proposed model is used for optimal management of the absorption chiller, the thermal efficiency of the plant increases significantly, doubling the solar contribution. As a result, the gas consumption of the solar cooling plant is halved and the total cost of air conditioning the building decreases by 16%.

1. Introduction

International Energy Agency estimates that a third of CO_2 emissions come from buildings. If the population continues increasing, energy needs could rise to 50% in 2050 (International Energy Agency, 2013). New energy-saving regulations and growing awareness in society lead to the need for decreasing energy consumption in buildings (European Commission, 2018). In addition, the cooling consumption of buildings represents a considerable fraction of total energy consumption in the world (Santamouris et al., 2004). Therefore, emphasis must be placed on reducing cooling needs and meeting the remaining needs with highly efficient equipment powered by renewable energy sources.

Considering that peak cooling demand occurs when solar energy potential is at its highest level, solar cooling would be an attractive alternative to reduce the environmental impact of conventional cooling systems (Bataineh and Taamneh, 2016). However, a review of the studies carried out shows that, although the technology exists in the market, its implementation in real buildings is still scarce. One of these limitations is the control of the absorption chiller operation (Ahn et al., 2019). In addition, the hybridisation of these chillers with solar cooling systems leads to changes in their performance due to the different characteristics of solar energy compared to auxiliary energy sources. However, many efforts have been made to discuss the performance of these systems from different points of view, including energy (Karki et al., 2019), economic (Leckner and Zmeureanu, 2011) and environmental impact (Chen et al., 2020). Therefore, different methodologies have been used to optimise operation

* Corresponding author.
E-mail address: alberto.cerezo@uca.es (A. Cerezo-Narváez).

https://doi.org/10.1016/j.egyr.2022.02.128

Nomenclature

A	Area (m^2)
BMS	Building Management System (-)
$C_{p,w}$	Specific heat of water (J/kg K)
CAP_{nom}	Nominal power expressed in EUROVENT conditions (W)
$Cold_{real}$	Cooling capacity in real operating conditions (kW)
$Cold_{nom}$	Cooling capacity in nominal operating conditions (kW)
$ConGasH_{real}$	Gas consumption in heating mode in real operating conditions (kW)
$ConGasH_{nom}$	Gas consumption in heating mode in nominal operating conditions (kW)
$ConElecH_{real}$	Electrical consumption in heating mode in real operating conditions (kW)
$ConElecH_{nom}$	Electrical consumption in heating mode in nominal operating conditions (kW)
$ConGasC_{real}$	Gas consumption in cooling mode in real operating conditions (kW)
$ConGasC_{nom}$	Gas consumption in cooling mode in nominal operating conditions (kW)
$ConElecC_{real}$	Electrical consumption in cooling mode (kW)
$ConElecC_{nom}$	Electrical consumption in cooling mode in nominal operating conditions (kW)
COP	Coefficient Of Performance (-)
COP(t)	Relationship between supplied and consumed power (-)
DDt'	Adapted Characteristic Equation model (-)
DEAM	Double Effect Absorption Machine (-)
DHW	Domestic Hot Water (-)
EER	Energy Efficiency Ratio (-)
EES	Engineering Equation Solver (-)
EHP	Electric Heat Pump (-)
EPBD	Energy Performance of Buildings Directive (-)
F_{CAP}	Correction factor that corrects the cooling capacity based on the operating temperature (-)
F_{CON-1}	Correction factor of the efficiency curve as a function of the condenser inlet temperature (-)
F_{CON-2}	Correction factor of the efficiency curve as a function of the partial load factor at which the machine works (-)
FDD	Fault Detection and Diagnosis (-)
GEHP	Gas Engine Heat Pump (-)
GNA	Adapted Gordon-Ng model (-)
H_2O	Water (-)
$Heat_{real}$	Heat capacity in real operating conditions (kW)
$Heat_{nom}$	Heat capacity in nominal operating conditions (kW)
	$HTG(t)$ Generator temperature (°C)
HVAC	Heating, Ventilation and Air Conditioning (-)
LiBr	Lithium bromide (-)
$\dot{m}_{gen}$	Flow rate (kg/s)
$\dot{m}_{cond}(t)$	Fluid flow rate through the condenser (kg/s)
m_{rec}	Bypass flow (kg/s)
m_w	Water flow (kg/s)
MCp	Thermal mass (J/K)
MCp_{on}	Thermal mass found in the generator (J/K)
MCp_{off}	Thermal mass in the generator taking into account the calorific coefficient of that mixture at stop (J/K)
MPR	Multivariate Polynomial Regression model (-)
NG	Natural gas (-)
NZEB	Nearly Zero Energy Building (-)
p_{CAPi}	Coefficient that defines the correction curve (-)
p_{CONi-j}	Coefficient of the fit curve for the correction factors (-)
PCM	Phase-change material (-)
PLR	Part load ratio (%)
$Q_{cond}(t)$	Power supplied by the condenser (W)
$Q_{cooling}$	Cooling power delivered by the machine (W)
$Q_{ext}(t)$	Necessary heat to be dissipated from the generator for the correct operation of the absorption machine (W)
$Q_{gen,nom}$	Nominal power of the generator (W)
$Q_{RECOVERY}$	Heat recovery from cooling system of engine (kW)
$RecQH_{real}$	Heat recovery in heating mode in real operating conditions (kW)
$RecQH_{nom}$	Heat recovery in heating mode in nominal operating conditions (kW)
$RecQC_{real}$	Heat recovery in cooling mode in real operating conditions (kW)
$RecQC_{nom}$	Heat recovery in cooling mode in nominal operating conditions (kW)
RER	Renewable Energy Ratio (-)
SEER	Seasonal Energy Efficiency Ratio (-)
SCOP	Seasonal Coefficient Of Performance (-)
SCR	Solar cooling ratio (-)
SHF	Solar heat fraction (-)
τ_{enf}	Time constant (s^{-1})
τ_{on}	Generator start time constant (s^{-1})
τ_{off}	Generator shutdown time constant (s^{-1})
T_{dr}	Outdoor dry-bulb temperature (°C)
T_{wb}	Outdoor wet-bulb temperature (°C)
$T_{evap,i}$	Inlet water temperature to the evaporator (°C)
$T_{evap,o}$	Outlet water temperature from the evaporator (°C)
T_{on}	Starting temperature of the generator (°C)
T_g	Generator temperature (°C)
$T_{g,min}$	Minimum working temperature in the generator (°C)
$T_{gen,i,nom}$	Nominal operating temperature of the generator (°C)
$T_g(t\text{-}\Delta t)$	Generator temperature at a previous time (°C)

$T_{gen,i}(t)$	Fluid temperature at the generator inlet (°C)
$T_{gen,o}(t)$	Fluid temperature at the generator outlet (°C)
$T_m(t)$	Average fluid temperature between the inlet and outlet to the generator (°C)
$T_{cond,i}$	Inlet water temperature of the dissipation loop (°C)
$T_{cond,o}(t)$	Condenser outlet temperature (°C)
T_{irec}	Inlet water temperature of recovery loop (°C)
T_{orec}	Outlet water temperature of recovery loop (°C)
T_{iw}	Inlet water temperature (°C)
T_{ow}	Outlet water temperature (°C)
$T_{LIM-REC}$	Minimum outdoor temperature to put on recovery system of GEHP (°C)
$T_{SETPOINT}$	Set point temperature (°C)
TRNSYS	Transient System Simulation Tool (-)
U	Overall heat transfer coefficient ($W/m^2 K$)
UA	Overall heat transfer coefficient per generator area (W/K)
UA_{on}	Overall transfer coefficient through generator area at start-up (W/k)
UA_{off}	Overall heat transfer coefficient through the generator area at stop (W/k)

strategies (Araújo and Silva, 2020) and system configurations,10 to improve the performance of hybrid solar cooling systems.

Absorption chillers are being used in most of the solar cooling systems in operation today (Prieto et al., 2019). The typical range of cooling capacities for commercial absorption chillers is from 5 to 1500 kW (Xu and Wang, 2017). Thermal compression of the refrigerant is achieved by using a liquid refrigerant (absorbent) solution and a heat source, which replaces the electrical consumption of a mechanical compressor. There are two configurations for absorption systems: single effect and double effect. The main difference between them is the operation temperature, which is lower in single effect ones. In addition, double-effect absorption chillers may have a higher COP due to possible energy recovery (Wang et al., 2017).

As mentioned above, control of the absorption machine operation is required to optimise system performance. In first, the operation of the system should be controlled. For example, the weak point of this solution is the risk of crystallisation (Jradi and Riffat, 2014). For that, the dissipation water temperature must be controlled. On the other hand, a solar cooling plant requires efficiency control to maximise the renewable contribution. Modelling can be considered an excellent solution for operating this chiller (Jradi and Riffat, 2014) and predicting solar production (Rivarolo et al., 2013). When modelling the performance of an absorption chiller machine, the coupling between the device and the solar collector field must not be forgotten. This coupling condition consists of the thermal power produced by the solar field being greater than or equal to that required by the absorption chiller generator (Sarabia Escriva et al., 2011). This issue has also been studied by Evola et al. (2013), and they highlighted the relevance of this problem for absorption chillers. In addition, the high mass of the internal components and the accumulation of fluids inside the vessels usually make the transient period longer than in the case of mechanical compression. Therefore, authors as Sebastián et al. (2021) demonstrated the need for well-characterised inertia models in short time steps (less than 30 min) for decision making in solar cooling plants. Previous works showed the existing research gap in the literature on the lack of solution about the coupling between the absortium chiller model and solar sources.

Shirazi et al. (2018) conducted a comprehensive literature review on the current status of this technology and its modelling. This work showed the lack of experimental validation of many publications and how the modelling streams are either TRNSYS types (Klein, 2010) or models with detailed thermodynamic processes. According to Martínez et al. (2016), there are primarily two approaches to model an absorption chiller. The first option (detailed models) consists of adding all thermodynamic characteristics of the chiller into a set of simple algebraic equations. The second option (simplified models) uses heat transfer coefficients (U), heat exchange areas (A) and working fluid characteristics to simulate machine behaviour. In this second case, mass and energy balance equations are established for each cycle that considers the different streams that converge in each component, defining their thermodynamic behaviour. Table 1 summarises a review of absorption chiller characterisation models.

The most recurrent option in the reviewed literature is to use simplified models for the characterisation of absorption chillers. However, the methodologies presented do not clearly explain the formulation that allows the integration of manufacturer data or the thermal parameters obtained through experiments into these models. For example, it does not appear how to consider a machine of better performance and therefore higher cost than another of low performance. The existing literature (Nikbakhti et al., 2020) also presents modelling proposals for absorption chillers but does not provide a solution for their integration with solar systems, avoiding connecting them to the management system for optimal operation. The present work provides a simplified model based on characteristic parameters that can be identified from manufacturer or experimental data. In addition, this proposal solves the integration with renewable sources in a simple way.

Table 1 also shows how simplified models could present a lack of cohesion between the experimental data, the actual performance of the machines, and the input/output data of these models. To close this gap, seasonal values can be used as the key performance indicator to evaluate the acceptability of the estimation or the real benefits of facilities (Kylili and Fokaides, 2015). For example, the most frequent are the thermal efficiency of the chiller or the percentage of renewable contribution using the RER of the building (Nikbakhti et al., 2020). Recent publications, such as Bilardo et al. (2020), discuss the limitations of using simulations with the current state of models. Simplified models remain the most compatible with transient energy performance simulation tools (Castro et al., 2020). Many of these renewable technology models appear in the databases of TRNSYS (Klein, 2010) or EnergyPlus (Anon, 2018). Although the models before have not been updated for more than 20 years, and they are not taking into account the progress of these technologies. These simplified models characterise HVAC systems by the use of performance curves (Ray et al., 2021). Sánchez Ramos et al. (2019) demonstrated the validity of simplified models based on operating curves for equipment characterisation without high thermal inertia, such as natural gas heat pumps. However, these proposals should not be used for real-time optimal control due to their low accuracy in simulation with short time steps (Lubis et al., 2018). Nevertheless, the scientific community is accepting the use of simplified models if their estimation of main key performance indicators is acceptable.

According to the above, there is a lack of research on this topic. However, this research addresses the experimental quantification

Table 1
Review of absorption chiller characterisation models.

Reference	Year	Type of model	Summary
Martínez et al. (2016)	2016	Simplified	They proposed a simulation model in the EES software environment that considered the internal characteristics of the absorption chiller. With this information, a weak solution flow rate and UA values for each chiller heat exchanger were estimated to reproduce consistent results that agreed with the available experimental data.
Florides et al. (2002)	2002	Simplified	They used the TRNSYS software environment using a new Type to simulate this system. The authors stressed the importance of providing measured input data, which the model should consider in order to account for measurable data.
Zhao et al. (2020)	2020	Detailed	They proposed a detailed model from which the different elements of a refrigeration machine could be extracted. The elements were modelled by their thermodynamic formulation.
Chen et al. (2017)	2017	Simplified	They developed a TRNSYS type, which was validated with experimental data. This comparison was performed by exciting the model with the input data measured on the experimental setup. The authors commented on the difficulty of establishing a proper definition of the absorption machine based on models proposed in the literature.
Yu et al. (2019)	2019	Simplified	They worked with the dynamic characterisation of the COP of an absorption machine in an experimental facility. The measured and estimated instantaneous results were different. However, the estimation of seasonal performance was acceptable. This work consolidates the idea that simplified models are required but considering the dynamics of these machines.
Ibrahim et al. (2017)	2017	Simplified	They studied an experimental facility attached to a building with thermal storage. Their absorption system model was limited to assessing the machine COP as a function of operating conditions. The authors commented on the non-validity of the model on a shorter time basis, highlighting the need to consider the start-up and shutdown dynamics of this type of chillers.
Castro et al. (2020)	2020	Detailed	They used a detailed modelling pathway to perform sensitivity studies for enabling the optimal design of this type of chillers (manufacturer). They obtained the requirements for the future modelisation and the monitoring system to develop an internal control for these chillers.

of this control and management. For this purpose, the first goal of this research is to develop an inverse model for the absorption chiller, which enables its calibration with real operating data. It should be noted that the coupling between the plant elements (without optimising) has been solved in previous research (Gallego et al., 2020). In this context, the accuracy of the model is a critical parameter, as it is linked to the ability to analyse the transient effect of these technologies. Therefore, this is considered a point of great importance in order to optimise their operation. Another key element in a solar cooling plant is the absorption chiller (Shirazi et al., 2018), as it is connected to the natural gas consumption of the auxiliary boiler and the renewable energy source. Consequently, if it is not optimally operated, the solar contribution decreases significantly (Jalalizadeh et al., 2021). Recent reviews, Settino et al. (2018) have concluded that the validation of an absorption technology in a controlled environment is different from that of the same technology but coupled to a solar cooling plant. It is because solar plants are exposed to many variations in renewable resources, which generates a greater need for control in a short time, as Song et al. (2020) proved. Traditionally, linear and nonlinear models have been considered the best option (Shirazi et al., 2018) to calibrate using experimental data. Both are based on statistical errors when comparing real production with theoretical statistical production (Gallego et al., 2020). At present, artificial intelligence techniques are undergoing massive development to analyse complex technologies such as solar systems (Mao et al., 2020).

In this context, Amiri Rad and Davoodi (2021) and Ali and Ratismith (2021) worked with simplified models, in which these systems are coupled into higher-order entities (in their case, thorny plants). Sharafi et al. (2015) optimise this renewable ratio and conclude that transient models with low computational overhead are needed to achieve seasonal results and generate robust transient results such as required peak powers. This research proposes a new model that combines equipment performance curves from experimental data provided by manufacturers with "in situ" experiments that include fast start up and shut down effects for the absorption chiller. Nevertheless, these authors did not solve the model for the coupling between performance curves and transient effects.

Furthermore, the second goal of this research is to contribute to the existing literature by proposing an optimised model for the characterisation of absorption chillers coupled to solar systems. In addition, the inverse model is integrated into the management system as a predictive control to support the operator decision. The validation of the model is based on an experimental installation of solar cooling in a Fresnel collector attached to a university building for air conditioning. An entire solar cooling plant is operated to achieve these research goals. These experimental results are interesting and will be fully analysed throughout the paper.

2. Method

This research intends to couple an absorption chiller with the energy management model of a solar cooling plant through an inverse model. This model is validated using a solar cooling plant. The experimental facility is coupled with a real building and operated in actual conditions. Furthermore, this research provides the identification, design and development of an inverse model for the chiller. In addition, a decision support system performs this coupling as a predictive control for the plant. Therefore, the main contributions of this paper are: the proposed model to characterise the absorption chiller coupled to the solar cooling plant, the experimental results obtained during the validation of the model, and the results linked with the application of the model as a predictive control for the plant.

Fig. 1 shows the context of this research: the renewable thermal production system with storage and the building that requires this energy for cooling. For this purpose, a double-effect absorption machine receives heat both from renewable resources and a backup boiler coupled to it. This support boiler operates in accordance with the availability of renewable resources and the working instructions of the absorption machine. Therefore, if the control management is not performed intelligently to maintain the operating instructions of the absorption machine, uncontrolled entry from the natural gas support system may occur. For this reason, a characterisation model is needed to infer the response of the absorption machine to variations in building cooling

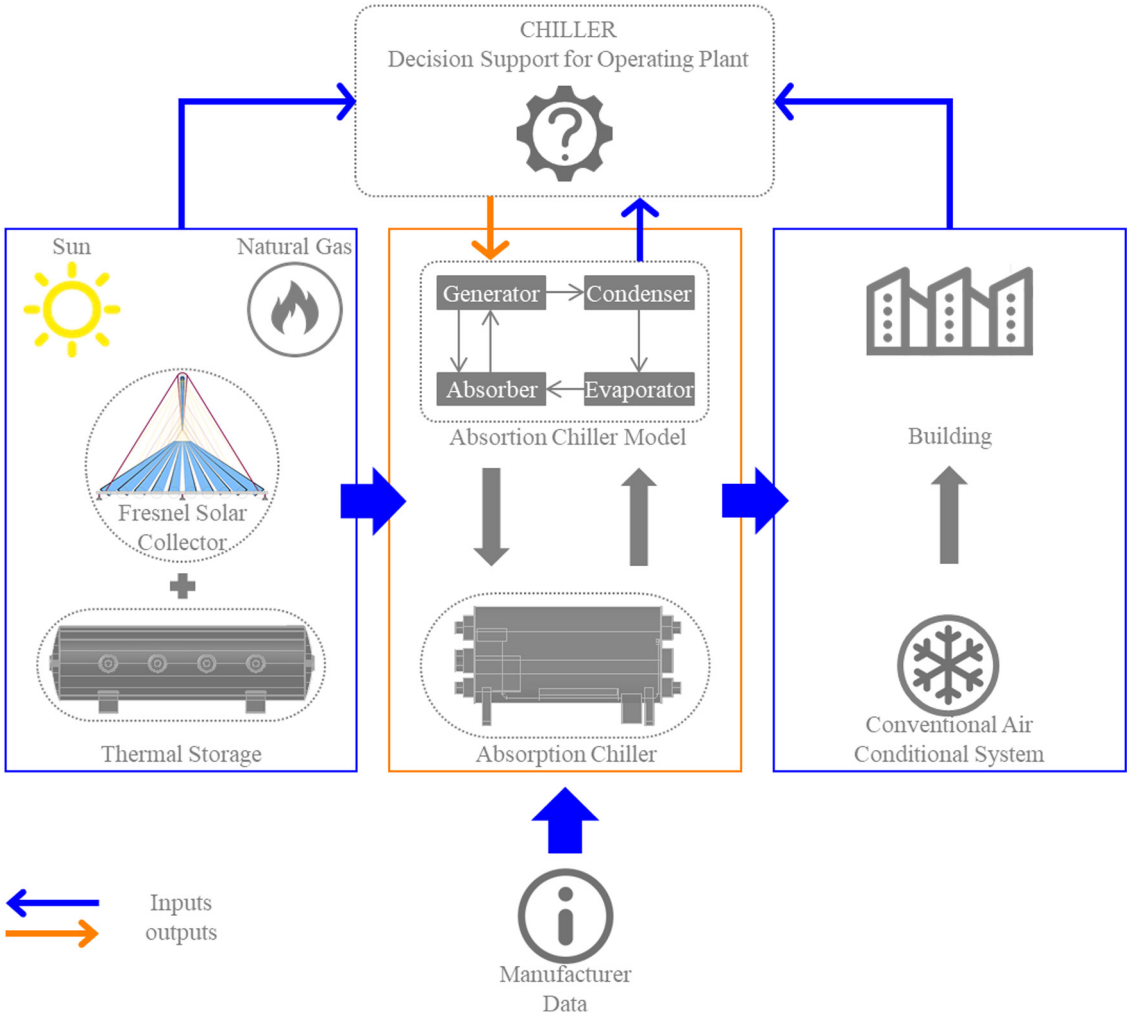

Fig. 1. Scheme of the methodology.

needs and renewable resources. Consequently, gas consumption can be minimised and the use of renewable resources maximised because the inverse model allows deciding the best command to operate the absorption chiller. The proposed model is validated using available experimental data of real system operation.

As mentioned above, a model of the behaviour of the absorption machine from the behaviour curves is defined. Both working temperatures and parameters of the absorption machine are used as variables. The developed model requires data from the manufacturer (curves and nominal parameters) and flow rates and temperatures of the input flows (solar generator, dissipation system and building cooling circuit). Then, the model estimates the outlet temperature of each flow and the possible gas consumption required, according to the control signal received (predictive control). The inverse model is executed every 30 min to evaluate the operation strategy for the absorption chiller. The inputs and outputs of the model will be detailed in the next section.

3. Experimental solar cooling plant

3.1. Overview of the solar cooling plant

A pilot solar cooling plant was developed to test a cost-efficient alternative to grid power consumption, taking advantage of the high insolation levels in the Spanish region of Andalusia. The plant was coupled to an existing compression chiller cooling system. Both systems are located on the roof of a university building. Its main components are summarised in Fig. 2. The main aim of this plant is to prove the feasibility of significantly reducing the high electrical energy consumption of buildings for air conditioning by using solar energy.

The plant has been operating since 2008. It has been tested and monitored during this period to obtain data to evidence the feasibility of the concept, refine the design and operating practices, and assess its potential economic and environmental value. The double effect absorption chiller (see Fig. 2 left) uses LiBr–H2O as a refrigerant. The generator is powered by the heat coming from a linear Fresnel solar collector (see Fig. 2 right), which is able to reach a water temperature of up to 180 °C, thanks to a solar tracking system implemented in its mirrors. If the solar field cannot reach the temperature required for the operation of the absorption machine, a PCM storage tank (see Fig. 2 centre) is available for use. The cooling capacity of the system is 174 (kW). The proximity of the Guadalquivir river provides the source of cooling water used in an open-loop since the river water temperature during the summer is about 27 °C. Fig. 3 shows the different subsystems within the plant that can be distinguished, which require a detailed description. Their synergy provides the energy direction of the plant design.

Table 2 shows the parameters that characterise the Fresnel solar collector. In addition, the Fresnel solar collector starts tracking the sun when direct solar radiance exceeds 200 W/m^2. This system is shown in detail in Fig. 4. The highest allowable temperature in the tube is 180 °C. If the temperature exceeds 190 °C,

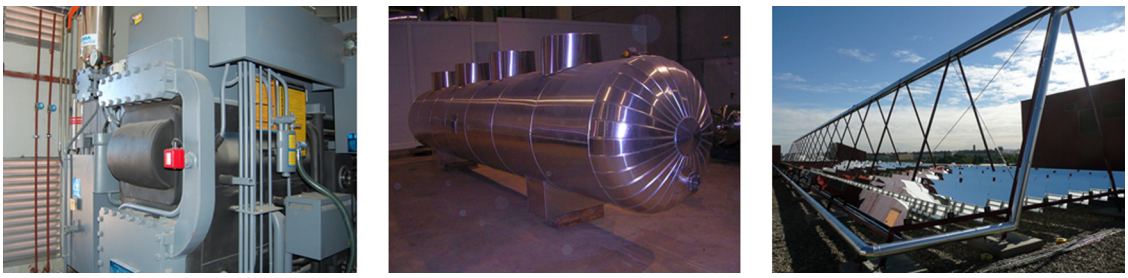

Fig. 2. Components of the solar pilot cooling plant installed at the Engineering School of Seville (Spain) (left: Absorption Chiller, centre: PCM Storage Tank, right: Linear Fresnel Solar Collector).

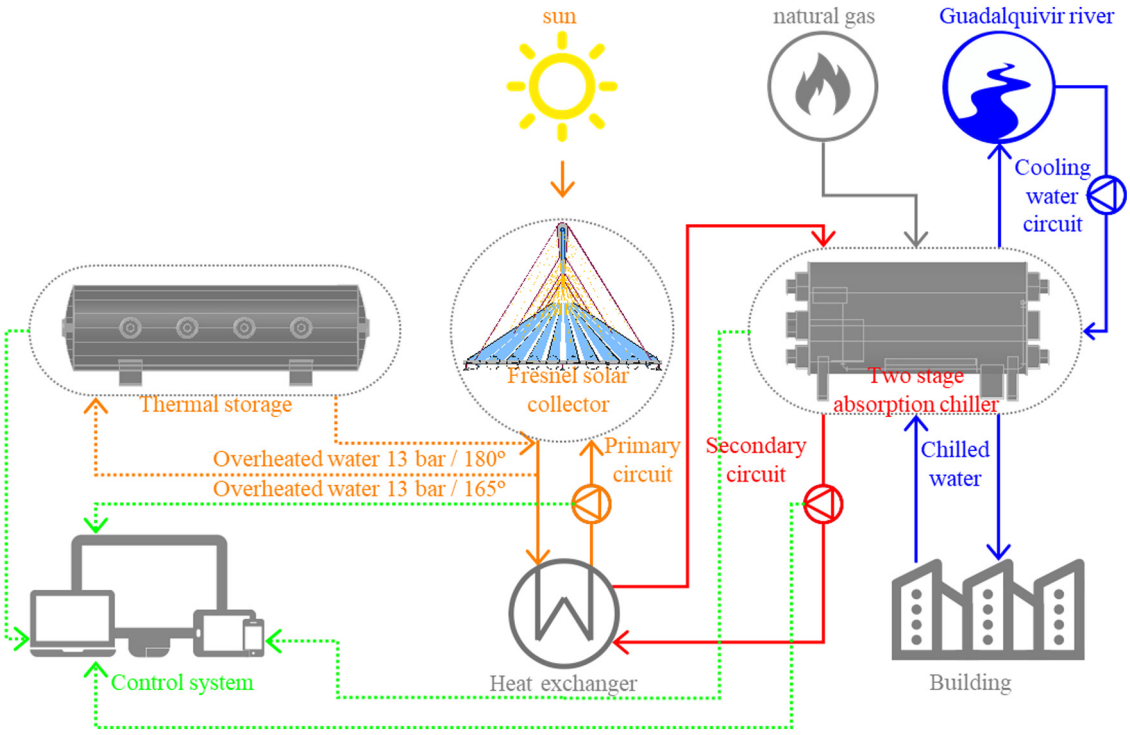

Fig. 3. Diagram of the pilot solar cooling plant installed at the Engineering School of Seville (Spain).

Table 2
Fresnel solar collector parameters.

Ground surface	512 m^2
Solar field	352 m^2
Orientation	East–West (azimut of solar collector is 18° from North)
Absorber tube length	64 m
Receiver height	4 m
Secondary width	0.3 m
Absorber tube model	SCHOTT PTR©70
Thermal fluid	Liquid water
Operating temperature	180 °C
Operating pressure	13 bar
Mirror dimension	2 × 0.5 m^2
Mirror reflectivity	0.92
Collector concentration	25

all mirrors are automatically turned upside down to protect the system. The temperature is controlled to be maintained at a set point which, in the case shown (see Fig. 4 right), was 170 °C, although it is normally 180 °C. For a water flow of 12 m^3/h, the average temperature gap between inlet and outlet was 7.2 °C, which corresponds to a solar thermal power of 100 kW. This power is used to provide heat to the chiller generator.

The Fresnel solar collector and the absorption chiller are connected through a 150 m long pipeline and a 6 m^3 PCM storage tank. This tank is 18 m long and 1.31 m in diameter. It is a shell and tube heat exchanger with a theoretical thermal storage capacity of 275.5 kWh, corresponding to a temperature range of 145–180 °C. The substance used in the tank is hydroquinone (3500 kg), with a melting point of 170 °C.

The absorption chiller of the plant only covers 30% of the total cooling needs of the building. However, it should be noted that this is a pilot plant. The absorption machine installed corresponds to the BROAD-BZH15 model, which has a nominal power of 174 kW and a theoretical COP of 1.34. The high-temperature generator receives hot water from the solar field, with a temperature range that is usually between 140–170 °C, with a nominal flow of 13 m^3/h. If the temperature is lower than 145 °C, the absorption machine starts the auxiliary system, which uses natural gas as fuel. The evaporator is an exchanger that cools the water from 14 °C to 7 °C with a nominal flow rate of 30 m^3/h. In the nominal operating regime, the temperature of the high-pressure generator is close to 145 °C, and most of the thermal power supplied to the machine comes from the solar collector water. The cooling capacity is maintained at around 135 kW (75% of its nominal capacity).

Fig. 4. Linear Fresnel solar collector installed at the Engineering School of Seville (Spain).

The plant runs in different operating modes. In Fig. 5, those used in the experiments performed during a full cooling season of the building (from May to October) are shown:

- Mode 1. Plant start-up. When direct solar irradiation is higher than 200 W/m2, the solar collector starts in recirculation mode. This recirculation is activated until the water temperature in the primary circuit is higher than 100 °C. At this point, Mode 2 is activated.
- Mode 2. PCM tank preheating. The solar loop opens, and water flows into the PCM tank. The thermal storage system is discharged by heating the water until it reaches a temperature higher than 155 °C.
- Mode 3. Chiller start-up. The absorption machine is turned on when the water temperature is higher than or equal to 155 °C. Then, the water access to the PCM tank is closed. On a typical day, the absorption chiller starts up at midday. When the water temperature of the solar collectors is enough (at least 155 °C), the control system opens the valve, allowing the generator to preheat. However, if the generator temperature drops below 145 °C, the natural gas burner starts up. It should be noted that the internal control of the chiller system prioritises the temperature level of the generator. This is why it is so important to predict its temperature in order to minimise the use of the gas burner.
- Mode 4. Energy storage. If the outlet temperature of the solar collector is higher than 165 °C or the cooling needs of the building decrease, the PCM tank opens to be charged with the excess heat from the solar collector.

There is also a Mode 5 that operates on weekend. The system is switched on to store heat in the PCM tank. For that, the water from the solar field is recirculated until it reaches 180 °C in a closed loop. At that point, access to the PCM tank is opened. This mode remains active as long as the inlet temperature to the PCM tank is 2 °C higher than the outlet temperature.

On the other hand, it can be noted that the chiller start-up is possible before Mode 3 is activated. For this purpose, the support of the gas boiler is required. It is usually used in the early and late afternoon. This additional option is a further advantage to dispose of a model for predicting the behaviour of the chiller that improves its performance. Amiri Rad and Davoodi (2021) conclude how critical the operation of absorption chillers is when different energy sources are involved. In the case of this research, the internal control of the chiller attempts to ensure stable performance by operating the auxiliary boiler when the conditions of the renewable energy source vary.

3.2. Description of test plan and fault detection and diagnosis

To develop the test plan and fault detection and diagnosis (FDD), the plant was operated and data was recorded for the results evaluation. From this point of view, two options were considered:

- Type 1: Normal operation. The system operates in nominal values and automatic mode, satisfying the cooling/heating demand according to operating conditions.
- Type 2: Parameter deviation. One or more parameters that are available to researchers are modified, such as flow and temperature setpoints, energy management modes of the absorption machine, valve position to force an operating mode, weekend operation to reduce load, etc.

In the test plan and FDD, Type 1 experiments are performed from Monday to Friday. These are used to evaluate the efficiency of the installation and its equipment in normal operation, check the correct operation of all the elements (equipment, control system and strategies) and finally provide information to achieve possible improvements in both the elements and the whole. Type 2 tests are performed from Saturday to Sunday. The purpose of these is to operate the equipment at different points in order to obtain its operating curves. In this regard, it should be emphasised that the test plan and FDD should include several parameter deviation tests where several setpoint values and modes could be scanned on the same day.

In particular, the following parameters are analysed to characterise the operation of the double effect absorption machine: absorption machine inlet and outlet temperatures in all circuits; flow rates through the absorption machine in all circuits; natural gas consumption; exhaust gas outlet temperature; and percentage of CO2 in the exhaust gases. These last two parameters are used to verify the good performance of the natural gas burner.

In this context, the behaviour of the machine was studied for these nominal flow rates: cold water flow rate (30 m3/h), hot water flow rate (14.5 m3/h), condensing water flow rate (36.6 m3/h) and solar circuit water flow rate (7.6 m3/h). A partial load analysis was also performed by taking flow values of $\pm$ (25, 50, 75) %. In this way, how the COP varies at different loads was studied, comparing the results obtained with the values provided by the manufacturer.

From the analysis of the days of operation in cooling mode, the following findings can be taken:

- The collector operated with an average daily efficiency of more than 30%, reaching values around 37%.
- The average pipe loss rate was 16.47%. This value is high due to the existence of thermal bridges.
- The average solar factor obtained in the cooling period was over 60%, due to the cold starts and the direct radiation decrease in the late afternoon. The solar factor even dropped to 50% of previous values on cloudy days. Further details of these results are discussed in Section 5.1.

In addition, the most probable measured results when the machine operated at 100% load being powered by the renewable resource were as follows: a cooling capacity of 174.4 kW was

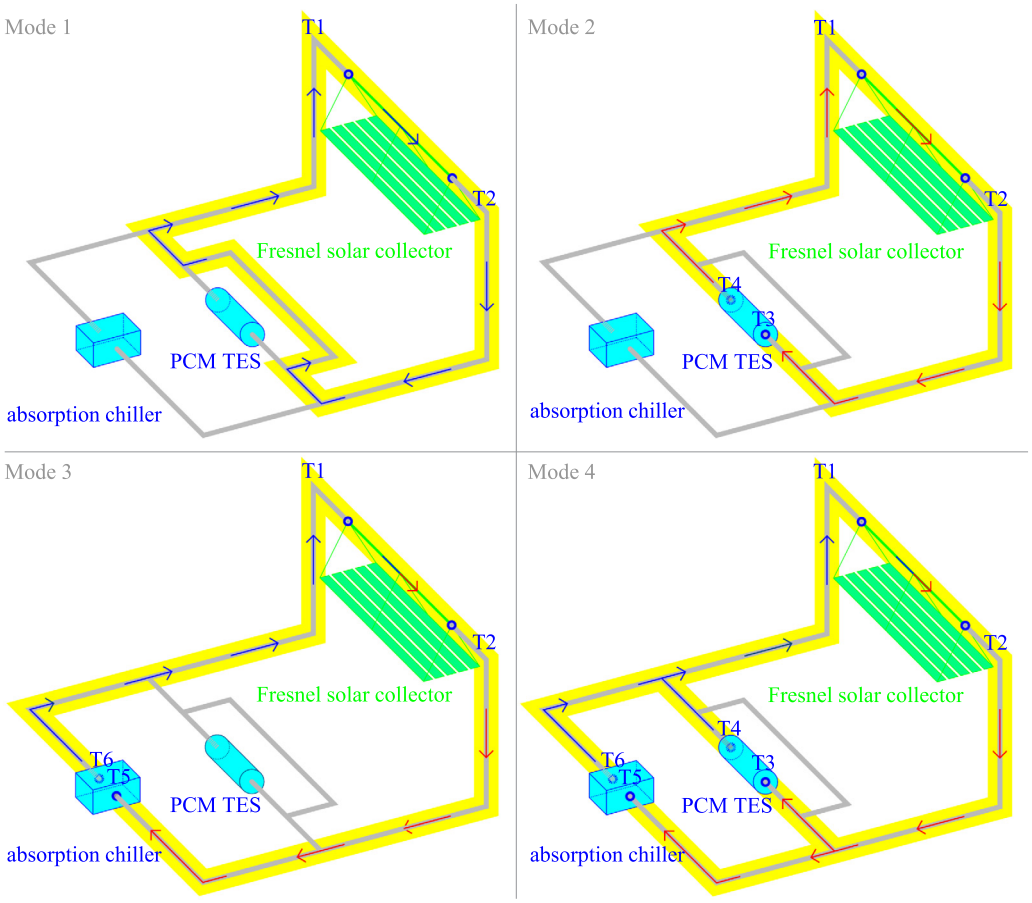

Fig. 5. Operation modes of the pilot solar cooling plant.

delivered, with the condenser dissipating a capacity of 296.4 kW. Under these conditions, the efficiency of the machine was 1.34.

After the most relevant Type 1 findings have been shown, Type 2 ones are now considered. For this purpose, the failures that occurred in the solar cooling plant during a period of operation of 2 years are analysed (a first year of commissioning of the experimental installation and a second one in which the results presented in this work were carried out). To this end, a database was set up in which 433 orders were collected during operation, making it possible to know the place where they occurred, the start and end date and the type of order. Among all of them, 133 errors were distinguished, which can be divided according to the type of error, the zone in which they occurred or the equipment from which they were produced.

Fig. 6 shows the frequency of faults divided by type. In the absorption solar cooling plant, the most frequent ones were the control system with 30.75%, mostly due to errors in the data acquisition system or in the reading/writing of signals. The next most frequent faults were electromechanical, mostly from pumps and solenoid valves, with 28.50%. These were followed by exclusively electrical faults in protections and other switchboard elements with 15.75%. The errors classified as "Others", with 12.00%, corresponded to errors related to issues such as corrosion, insulation, low battery in equipment, broken mirrors, etc.

Fig. 7 shows the frequency of shutdowns and faults recorded in the solar cooling plant divided by zone. As can be checked, the zone where most errors occurred was the solar circuit, with 44.85%, as this is the zone of the installation with the highest technical requirements. In second place, the cooling circuit with a frequency of 18.38%, mainly due to errors in the start-up or shutdown due to low pressure in the cooling circuit. In third place, the control system, with a frequency of 13.97%, followed by those related to the machine room, the raw water circuit, the distribution panel, the heat circuit and, finally, the exhaust gases and the gas train.

Fig. 8 shows the frequency of shutdowns and faults recorded in the solar cooling plant divided by the equipment on which this occurs and, therefore, on which it will be necessary to act, in accordance with the contingency plan. To this end, the errors found are divided according to the equipment from which they occurred. The equipment with the highest number of failures was the Fresnel collector with a frequency of 24.81%, mainly due to connection issues with the control system, failures in the row motors and control failures in the mirror rows. This was followed by failures in the pipe installation, due to instabilities in pressure and flow levels, as well as the occurrence of leaks. In third place, the control system was with a frequency of 12.78%.

A corrective measure is formulated for each of the errors. Therefore, by way of example, each of the faults found in the double effect absorption machine (DEAM) are compiled in Table 3, supported by a brief description and the consequence of the fault, as well as the corrective measure applied.

4. Model

4.1. Description

Absorption machines are based on the principle of condensation and evaporation of a refrigerant to obtain heat or cold, as required. They are systems capable of generating cold from the use of a medium/high-temperature heat source. Fig. 9 shows the main elements that compose this type of machine. The heat

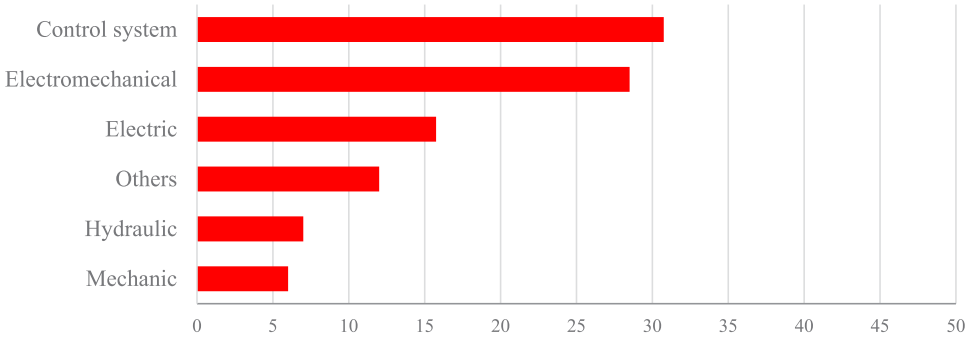

Fig. 6. Frequency of faults by type (in %).

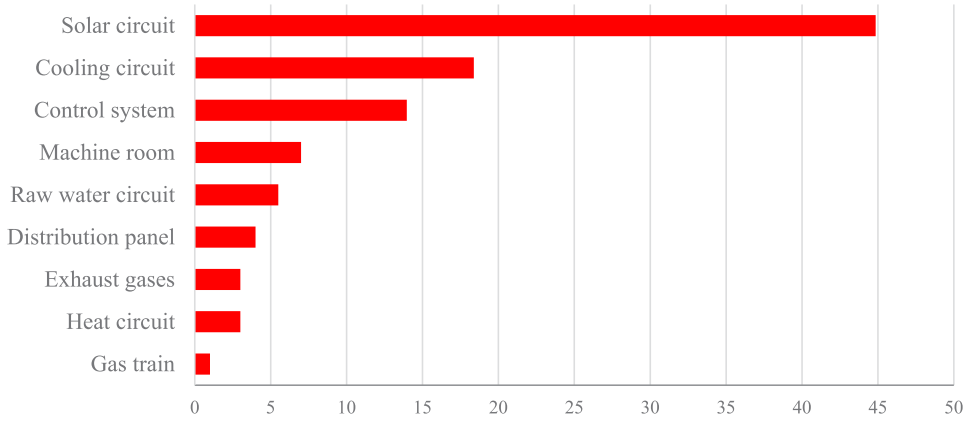

Fig. 7. Frequency of faults by zone (in %).

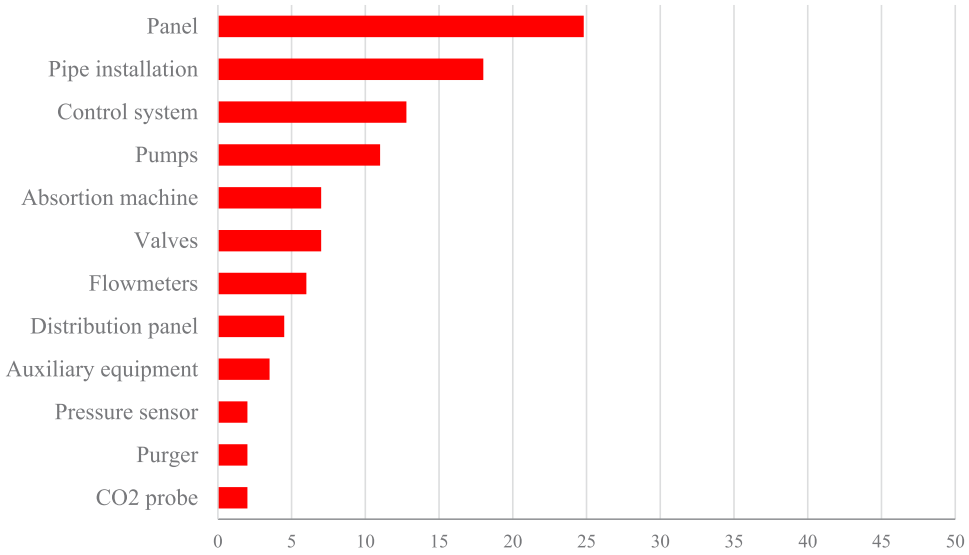

Fig. 8. Frequency of faults by equipment (in %).

flows (colour orange in Fig. 9) are explicitly shown in the machine model.

If the information provided by the manufacturer is analysed together with the experimental data obtained, then the behaviour of the machine under study can be simplified into three operating modes, as shown in Fig. 10. The orange line represents the temperature of the generator, whereas the blue one represents the temperature of the evaporator.

According to Fig. 10, Mode 1 corresponds to start up. The hot heat transfer fluid enters the generator to increase its temperature in this mode. However, this temperature (colour orange in Fig. 10) is not enough for the absorption machine operates. Once the temperature of the generator is adequate, the unit control starts the absorber–evaporator and condenser of the chiller sequentially. This Mode 2 refers to the nominal operation of the device, which ends with the shutdown mode. This model concerns the operation after the absorption machine stops due to the dilution effect. After turning off the device, the generator gradually cools down. Simultaneously, the evaporator produces cold water (blue colour in Fig. 10), although not at the nominal

Table 3
Fault detection and diagnosis.

Fault	Description/consequence	Corrective measure
Refrigerant level control system error	The refrigerant level in the DEAM exceeded one of the permissible limit values resulting in a shutdown	Removal of refrigerant from the circuit to prevent the limit from being exceeded
High evaporator pressure	The pressure in the DEAM evaporator exceeded the imposed limit, reducing the capacity to produce cold	Pressure relief valve
Excess temperature at the outlet of the DEAM in the cooling circuit	The outlet temperature of the DEAM in the cooling circuit is so high that instead of combating the heat load of the building, the conventional production system is penalised	Reprogramming, which involves shutting down the installation if this happens in order to prevent this from causing a penalty in the conventional system
No natural gas flow	Issues with the electric natural gas safety valve preventing the flow of fuel to the DEAM burner.	Reprogramming (electric natural gas safety valve incorrectly programmed)
No flame on burner	The DEAM burner fails to maintain flame after several unsuccessful reignition attempts resulting in shutdown.	Reprogramming of the electric natural gas safety valve, ensuring a minimum flow that allows the continuity of the flame
Irregular flow	The flow rate through the evaporator is below the required minimum, causing the equipment to shut down for protection	Repair of the hydraulic circuit due to large losses caused by a rupture
Incorrect seasonal mode of operation	Human error resulting from incompatibility between the DEAM configuration and the circuit valve control system	Reprogramming of the system that prevents DEAM actuation if the circuit is not set up for correct operation

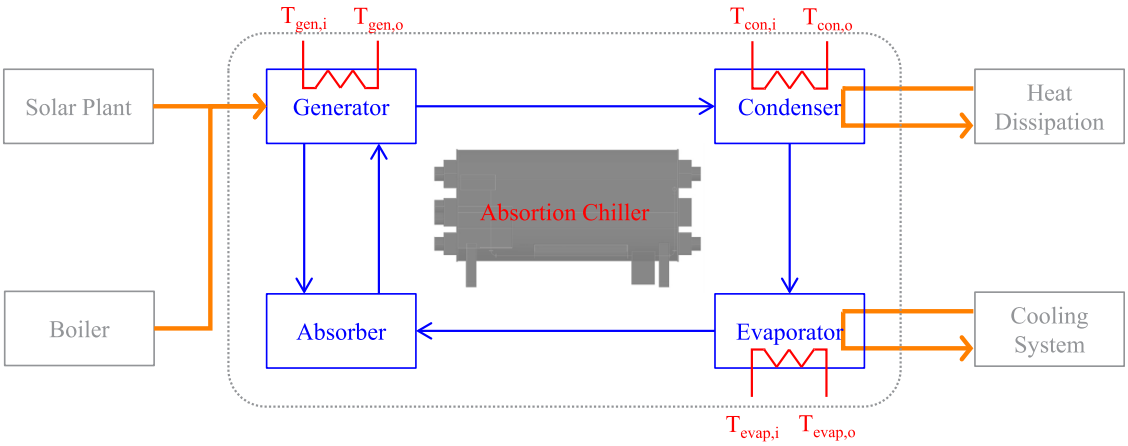

Fig. 9. Parallel scheme of the installation. (For interpretation of the references to colour in this figure legend, the reader is referred to the web version of this article.)

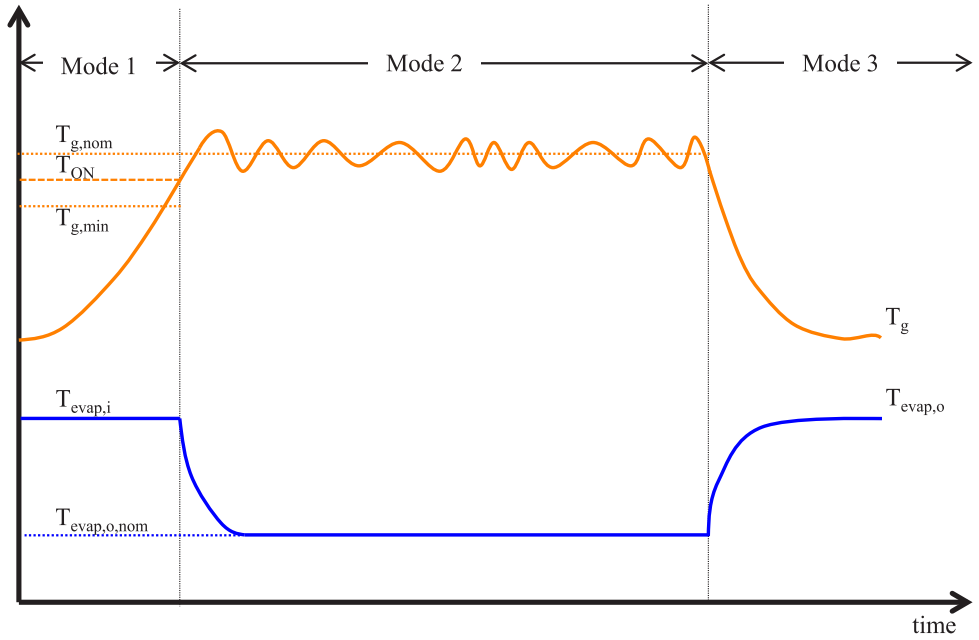

Fig. 10. Typical evolution of generator temperature in one cycle of machine operation. (For interpretation of the references to colour in this figure legend, the reader is referred to the web version of this article.)

temperature. This model has a second stage in which the absorption chiller has stopped producing cold water. Moreover, all the pumps are shut down.

In the following sections, each mode and its characteristics are formulated separately. Modes are an internal decision of the control unit algorithm. Each mode requires a different formulation. Based on the conditions of the previous instants, the algorithm decides which mode should be the one to execute the next timestep to be studied.

4.2. Mode 1: Start-up

Mode 1 is the characterisation model of the start-up mode. This model is based on the simplification of treating the generator as a capacity system whose temperature is Tg. Fig. 11 shows experimental data of temperatures (up) and thermal power (down) for a typical operating day during the three modes: start-up (yellow zone), regular operation (cyan zone) and shutdown (green zone). In addition, Fig. 11 (up) shows the high temperature of the system (generator, blue line) and the cold temperature of the system (outlet water of evaporator, red line). Finally, Fig. 11 (down) shows the thermal power linked with the solar production (blue line), the natural gas boiler (purple line), and the cooling production into the evaporator (orange line).

System starts up at approximately 10:00 AM, using the natural gas boiler. Then, Fig. 8 shows the nominal operating temperature of the generator, which is 140 °C, as indicated by the manufacturer. Because the minimum temperature is 120 °C, the starting temperature is around 130 °C. It has been assumed that the mode change occurs in the proposed model at that temperature.

Modes are based on the following balance of energy in the generator that Eqs. (1)–(3) show. It should be noted that the energy that enters the generator minus that which is extracted is used to increase the generator energy.

$$UA \cdot \left(T_m\,(t) - T_g\,(t)\right) - Q_{ext}\,(t) = MCp \cdot \frac{dT_g\,(t)}{dt} \tag{1}$$

$$\dot{m}_{gen} \cdot c_{p,w} \cdot \left(T_{gen,i}\,(t) - T_{gen,o}\,(t)\right) = UA \cdot (T_m\,(t) - HTG\,(t)) \tag{2}$$

$$T_m\,(t) = \frac{T_{gen,i}\,(t) + T_{gen,o}\,(t)}{2} \tag{3}$$

Where: $T_{gen,o}\,(t)$ is the fluid temperature at the generator outlet [°C]; $T_{gen,i}\,(t)$ is the fluid temperature at the generator inlet [°C]; $HTG\,(t)$ is the generator temperature [°C]; $T_m\,(t)$ is the average fluid temperature between the inlet and outlet to the generator [°C]; UA is the overall heat transfer coefficient per generator area [W/K]; $Q_{ext}\,(t)$ is the necessary heat to be dissipated from the generator for the correct operation of the absorption machine [W]; and MCp is the thermal mass [J/K] found in the generator, taking into account the calorific coefficient of that mixture. This parameter should be stable if the water flow rates through the generator are stable. On the other hand, $\dot{m}_{gen}$ is the flow rate of fluid that circulates through the generator [kg/s]; and $c_{p,w}$ is the specific heat of water [J/kg K].

The machine maintains this operating mode as long as its control signal is activated. The generator temperature in the previous simulation step is lower than the starting temperature (see Eq. (5)), and this start-up temperature is a variable not provided by the manufacturer. Experimentally, it has been deduced that the starting temperature is approximately at the midpoint between the nominal operating temperature of the generator and the minimum temperature at which operation is possible, as shown in Eq. (4).

$$T_{ON} = Average(T_{gen,i\_nom};\, T_{gen,i\_min}) \tag{4}$$

Where: T_{ON} is the starting temperature of the generator; $T_{gen,i,\_nom}$ is the nominal operating temperature of the generator; and T_{gen,i_min} is the minimum operating temperature of the generator.

$$If\ (HTG\,(t - \Delta t) < T_{ON}) \tag{5}$$

Where: T_{ON} is the starting temperature of the generator and $T_g\,(t - \Delta t)$ is the temperature of the generator at a previous time.

The inlet energy into the generator is used to increase the temperature of the generator (as shown in Eq. (6)). The evaporator does not produce cold, so the heat extracted is zero.

$$HTG(t) = \mathrm{HTG}(t-\Delta t) + \left[T_{gen\_i}\,(t) - HTG\,(t - \Delta t)\right] \cdot exp\left(-\frac{1}{\tau_{on}} \cdot \Delta t\right) \tag{6}$$

Where: τ_{on} is the generator start time constant [s^{-1}]. This time constant is the parameter from which the machine start up is characterised and approximated from the manufacturer data (see Eqs. (7)–(9)).

$$\tau_{on} = \frac{UA_{ON}}{MCp_{ON}} \tag{7}$$

$$UA_{ON} = \frac{\dot{m}_{gen} \cdot c_{p,w} \cdot \left(T_{gen,i}\,(t) - T_{gen,o}\,(t)\right)}{(T_m\,(t) - HTG\,(t))} \tag{8}$$

$$MCp_{ON} = \frac{\Delta t}{\left(\frac{1}{UA_{ON}}\right) \cdot ln\left(\frac{T_g(t) - T_{gen,i}(t)}{T_g(t-\Delta t) - T_{gen,i}(t)}\right)} \tag{9}$$

Where: UA_{ON} is the overall transfer coefficient through generator area at start-up [W/K]; and MCp_{ON} is the thermal mass [J/K] which is found in the generator, taking into account the calorific coefficient of the mixture at the start up.

The start-up time constant is identified using experimental data. For this purpose, start-ups are taken on different days. The time constant arises when the generator feedwater temperature difference (inlet minus outlet) is 37% of the initial temperature difference. This value of 37% has been taken from the proposal of Söderström (Mao et al., 2020). It should be noted that this value has been estimated at 44 min (minimum value of 38 and maximum of 49) using experimental data,. After that time, the absorption machine starts up the evaporator because the minimum working temperature in the generator $T_{g,min}$ has been reached. In turn, the thermal ignition mass takes a value of 7922 kJ/K (minimum value obtained from experimental data 7534 kJ/K and maximum of 8456 kJ/K).

In addition, solving Eqs. (1)–(3) allows obtaining the outlet temperature of the heat transfer fluid of the generator (see Eq. (10)). This variable can be measured and estimated by the model to be used for validation.

$$T_{gen,o}(t) = \frac{\left(\dot{m}_{gen} \cdot c_{p,w} - \frac{UA}{2}\right) \cdot T_{gen,i}(t) + UA \cdot HTG\,(t)}{\dot{m}_{gen} \cdot c_{p,w} + \frac{UA}{2}} \tag{10}$$

The model proposed is a function of the temperatures and flows involved in the thermal process. All the variables used can be measured in an installation. Due to the usual control of this type of facility, this variable can be employed to control them, as suggested by Martínez et al. (Yu et al., 2019).

4.3. Mode 2: Regular operation

When the generator temperature exceeds the starting temperature, the generator starts operating. At that moment, Mode 2 is activated (see Fig. 10), which is based on the curves provided by the manufacturer and considers that the generator temperature is constant and equal to the nominal temperature.

It is important to emphasise that this constant temperature operating mode is assumed for machines with a heat input via fuel (by direct flame). In this case, the operating curves do not depend on this temperature because the nominal operating mode

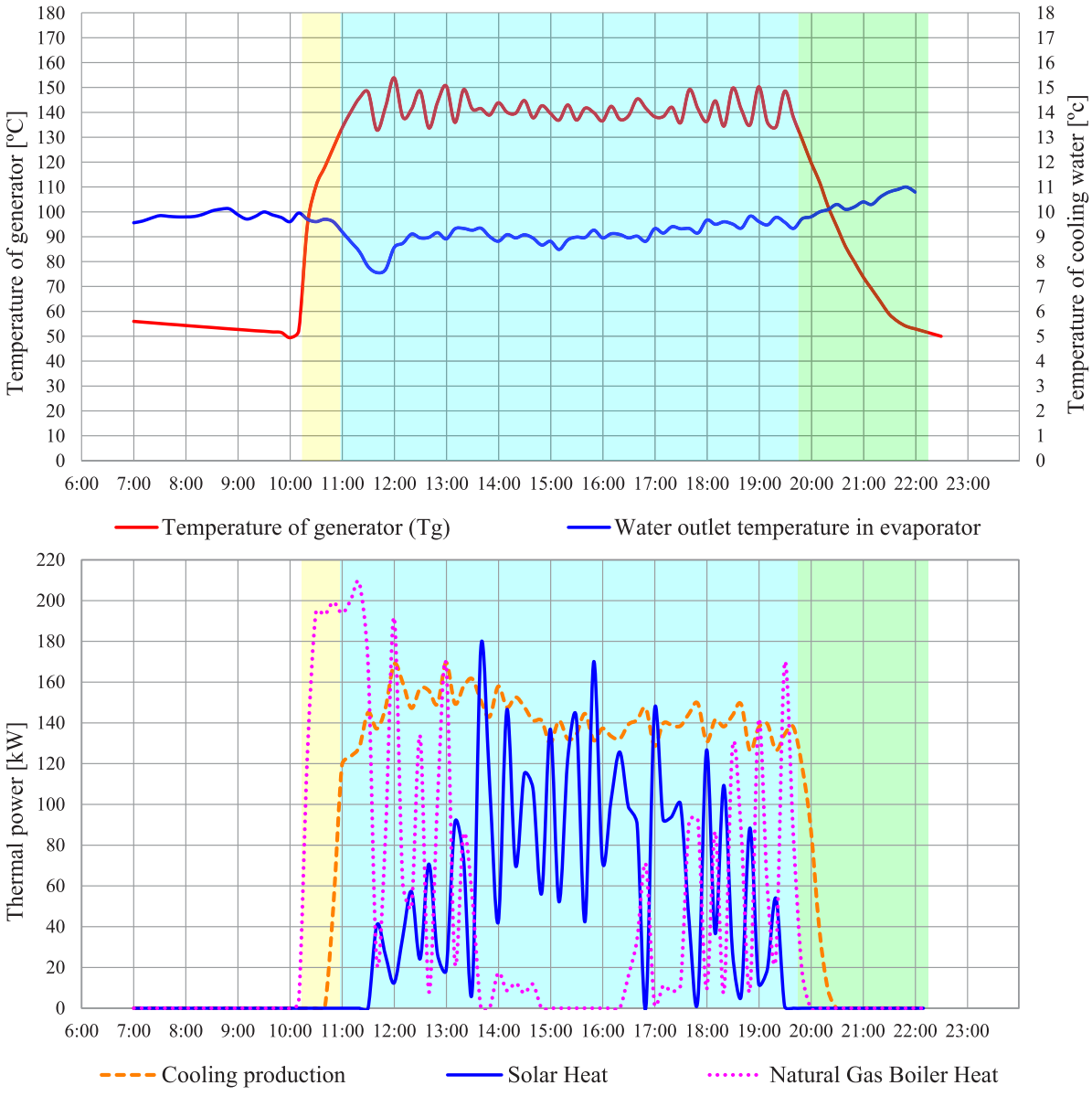

Fig. 11. Experimental data: Mode 1 (yellow), Mode 2 (cyan) and Mode 3 (green) Up: operation temperatures, Down: thermal power. (For interpretation of the references to colour in this figure legend, the reader is referred to the web version of this article.)

is assumed for it. If the machine is supposed to be connected to a renewable resource or to a recovered heat source (cogeneration), then the generator temperature will be assumed as a variable. In addition, the operating curves to be used will depend on it. Curves are used to define the thermal behaviour of the chiller in regular operation. This is usual for the energy characterisation of air conditioning systems (DOE, 2010).

First, cooling capacity $Q_{cooling}$ is defined as a function of its nominal capacity CAP_{NOM}, the outlet water temperature from the evaporator $T_{evap,o}$ and the inlet water temperature in the condenser $T_{cond,i}$, as shown in Eq. (11).

$$Q_{cooling}(t) = CAP_{NOM} \cdot F_{CAP} \cdot PLR(t) \tag{11}$$

Where: $Q_{cooling}$ is the actual delivered cooling capacity [W]; CAP_{NOM} [W] is the nominal power in Eurovent conditions (Anon, 2021); F_{CAP} is the correction factor that corrects the cooling capacity, which is based on the operating temperatures, both the evaporator outlet temperature $T_{evap,o}$ [K] and the generator temperature T_g[K]; and PLR is the partial load ratio [-].

Then, the correction curve for the cooling capacity F_{CAP} can be represented according to the function defined by Eq. (12), which depends on the operating temperatures.

$$F_{CAP} = p_{CAP1} + p_{CAP2} \cdot T_{\mathrm{evap},o}(t) + p_{CAP3} \cdot T_{\mathrm{cond},i}(t) + p_{CAP4} \cdot \left(T_{\mathrm{evap},o}(t)\right)^2 + p_{CAP5} \cdot T_{\mathrm{evap},o}(t) \cdot T_{\mathrm{cond},i}(t) + p_{CAP6} \cdot \left(T_{\mathrm{cond},i}(t)\right)^2 \tag{12}$$

Where: p_{CAPi} are the coefficients that define the correction curve; $T_{\mathrm{evap},o}$ is the evaporator outlet temperature [K]; and $T_{\mathrm{cond},i}$ is the condenser inlet temperature [K].

In addition, cooling production is directly linked to the flow rate and temperatures of the water in the evaporator, as shown in Eq. (13).

$$Q_{cooling}(t) = \dot{m}_{evap}(t) \cdot Cp_w \cdot (T_{evap,i}(t) - T_{evap,o}(t)) \tag{13}$$

Where $T_{\mathrm{evap},i}$ is the inlet temperature to the evaporator [K].

However, the cooling production requires a heat supply at the generator, and that supply must be compatible with the operating

temperatures and the PLR must be adjusted to cover the set point. This thermal consumption is calculated according to the following expressions (see Eqs. (14)–(17)):

$$Q_{gen}(t) = Q_{gen,nom} \cdot F_{CON-1}(t) \cdot F_{CON-2}(t) \tag{14}$$

$$T_{gen,o}(t) = T_{gen,i}(t) - \frac{Q_{gen}(t)}{m_{gen}(t) \cdot Cp_w} \tag{15}$$

$$FC_{CON-1}(t) = p_{CON1-1} + p_{CON1-2} \cdot T_{cond,i}(t) + p_{CON1-2} \cdot \left(T_{cond,i}(t)\right)^2 \tag{16}$$

$$FC_{CON-2}(t) = p_{CON2-1} + p_{CON2-2} \cdot PLR(t) + p_{CON2-3} \cdot PLR(t)^2 + p_{CON2-4} \cdot PLR(t)^3 \tag{17}$$

Where: $Q_{gen,nom}$ is the heat consumption of the generator; F_{CON-1} is the correction factor of the efficiency curve as a function of the condenser inlet temperature; and F_{CON-2} is the correction factor of the efficiency curve. This corrector is a function of the partial load factor the machine operates. In this context, p_{CONi-j} are the coefficients of the fit curve for the correction factors.

Next, the outlet temperature of the heat transfer fluid in the generator is cleared. This temperature will serve as a validation variable for the model, linking it with the solar system. It should be noted that from both the nominal cooling power and the nominal COP, the nominal flow rate of the generator can be deduced.

Finally, the power transferred to the condenser must be equal to the sum of the previous ones. The temperature at its outlet is calculated in the same way, as shown in Eqs. (18)–(20).

$$Q_{cond}(t) = Q_{gen}(t) + Q_{evap}(t) \tag{18}$$

$$T_{cond,o}(t) = T_{cond,i}(t) - \frac{Q_{cond}(t)}{m_{cond}(t) \cdot Cp_w} \tag{19}$$

$$COP(t) = \frac{Q_{evap(t)}}{Q_{gen}(t)} \tag{20}$$

Where: $Q_{cond}(t)$ is the required dissipation heat in the condenser; $T_{cond,o}(t)$ is the condenser outlet temperature; $\dot{m}_{cond}$(t) is the flow rate through the condenser, and $COP(t)$ is the relationship between supplied and consumed power.

The curves presented here depend on the manufacturer and the type of machine. The algorithm details the integration between the different inputs, parameters, curves and outputs of the model.

At this point, the problem is coupled. There are the minimum and maximum operating ranges for generator, condenser and inlet/outlet evaporator temperatures. The manufacturer sets these ranges. It is understood that they are to ensure the safety of the machine in case of crystallisation, overpressure, loss of vacuum, etc. If it is supposed that these ranges do not comply with the defined system of equations, then the internal control of the machine would regulate the load regime to modify the set point temperature.

4.4. Mode 3: Shutdown

Mode 3 is similar to Mode 1 (see Fig. 10), except that heat is lost to the generator for cooling. This cooling is performed with the heat transfer fluid of the generator without circulation but with the generator fan activated. The model provides this possibility in the downtime constant. This operating mode is maintained until the dissipation loop is stopped or the machine is turned on again.

In this mode, the machine is off. Eqs. (21)–(25) governing its behaviour are as follows:

$$Q_{evap}(t) = 0 \rightarrow T_{evap,o}(t) = T_{evap,i}(t) \tag{21}$$

$$HTG(t) = HTG(t - \Delta t) + \left[HTG(t - \Delta t) - T_{cond,i}(t)\right] \cdot exp\left(-\frac{1}{\tau_{enf}} \cdot \Delta t\right) \tag{22}$$

$$Q_{gen}(t) = \frac{MCp \cdot (T_{gen}(t) - HTG(t - \Delta t))}{\Delta t} \tag{23}$$

$$Q_{cond}(t) = Q_{gen}(t) \tag{24}$$

$$T_{cond,o}(t) = T_{cond,i}(t) - \frac{Q_{cond}(t)}{m_{cond(t)} \cdot Cp_w} \tag{25}$$

Where: τ_{enf} is the time constant [s^{-1}].

In this mode, the restriction is set by the condenser. If the condenser outlet temperature exceeds the maximum, the heat removed from the generator should be corrected. In that case, a new generator temperature would be calculated. It should be noted that the balance equations are analogous to those proposed in Mode 1, except that it is the condenser that evacuates the heat from the generator of the machine. Eq. (2), instead of a heat supply to the generator, would be an evacuation through the condenser. Eqs. (26)–(29) show the formulation of these parameters.

$$\tau_{OFF} = \frac{UA_{OFF}}{MCp_{OFF}} \tag{26}$$

$$UA_{OFF} = \frac{Q_{cond}(t)}{(T_m(t) - HTG(t))} \tag{27}$$

$$T_m(t) = \frac{T_{cond,o}(t) + T_{cond,i}(t)}{2} \tag{28}$$

$$MCp_{OFF} = \frac{\Delta t}{\left(\frac{1}{UA_{OFF}}\right) \cdot ln\left(\frac{HTG(t) - T_{cond,i}(t)}{HTG(t-\Delta t) - T_{cond,i}(t)}\right)} \tag{29}$$

Where: τ_{OFF} is the generator shut down time constant [s^{-1}]; UA_{OFF} id the overall heat transfer coefficient through the generator area at stop [W/K]; and MCp_{OFF} is the thermal mass of the generator when it is turning off.

As the condenser and evaporator have decoupled behaviours, each characteristic time constant is required independently. Following the procedure discussed for the start-up of the system, the cooling time constant is 115 min, with values ranging between 98 and 134 min. The thermal mass of the absorption machine has been taken as the equivalent thermal mass as if it were water. The value accepted is 8547 kJ/K (from experimental data, a minimum of 7862 kJ/K and a maximum of 8879 kJ/K have been obtained).

4.5. Identification of model

Thirty-three days of the cooling period of the building have been selected for this research. Several key performance indicators have been calculated for the solar collector, the absorption chiller, and the complete set for each day. The appendix shows the daily value of the incident solar energy in the solar field, the solar energy absorbed by the water in the collector, and the energy balance in the TES system. For the absorption machine, it shows the daily amount of heat supplied by the natural gas boiler and the solar field; the cooling produced by the system and delivered to the building collector; the average daily COP; and the percentage of solar contribution to total refrigeration produced (solar fraction). At last, the average efficiency performance of the plant is shown as the ratio between the cooling realised by the solar contribution and the total solar energy incident on the collectors. In addition, Table A.1 in Appendix shows these 33 days and their measured data.

On the other hand, 11 days have been taken from the sample presented in Table A.1 to estimate the coefficients of the model.

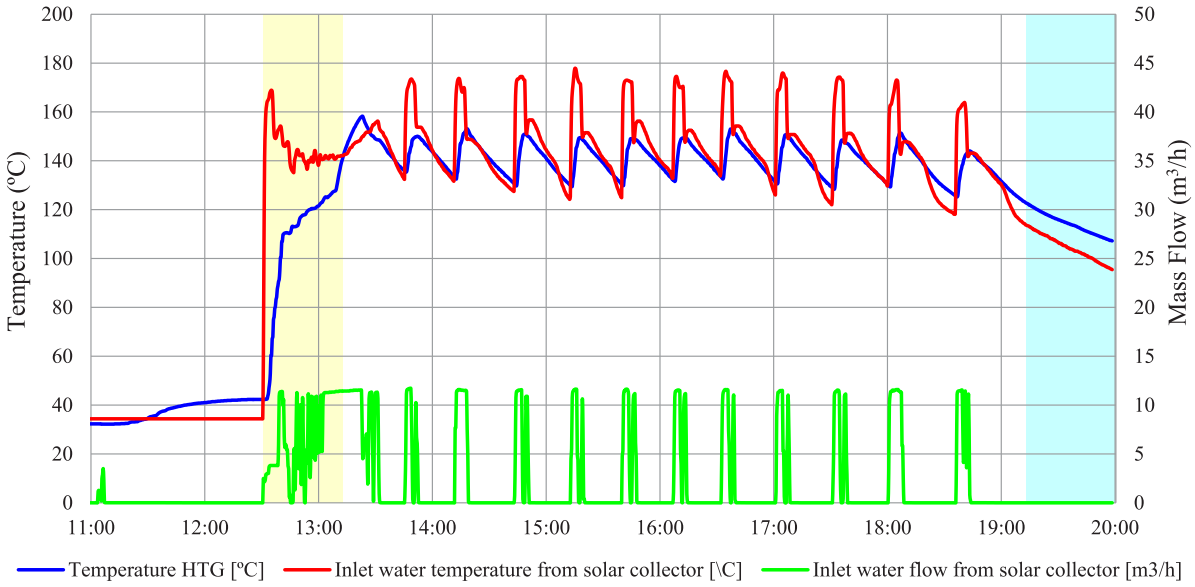

Fig. 12. Validation of the model: Detailed results. (For interpretation of the references to colour in this figure legend, the reader is referred to the web version of this article.)

They have been chosen at random and correspond to days 2–3, 5–6, 9, 12, 15, 22, 24, 27 and 31. The remaining days will be used for validation. The starts and stops of these days are employed to correct the values of the estimated time constants in Modes 1 and 3. Moreover, in Mode 2, the measured values of the thermal gas consumption, the thermal energy of the solar loop in the generator, the heat dissipated in the condenser, and the cold generated in nominal conditions are applied.

The model parameters are calculated from the experimental data at a step time of 10 min. These parameters are the heating and cooling time constants and the thermal mass of the generator. As explained before, these three parameters have been estimated using 11 days out of the 33 experimental days studied. For example, Fig. 12 shows one of the days chosen at random. The minimum generator temperature is 125 °C, which is reached 42 min (from 12:30 to 13:12 in Fig. 12) after starting the heating of the generator by passing water from the solar collector (see the yellow area in Fig. 12). After almost an hour of activation, the cooling has not concluded (see the cyan area in Fig. 12). It reaches the system shut down value after 122 min (from 19:10 to 21:12 in Fig. 12). At that moment, the temperature of the generator is below 45 °C.

On the other hand, the model requires identifying the coefficients of the operating curves. It should be noted that the data required to obtain these curves have been extracted from the information provided by the manufacturer. Fig. 13 shows the estimation of the coefficients of these curves and their comparison with the values of the manufacturer. In addition, Fig. 13 also shows the cooling capacity and EER as a function of outlet water temperature (X-axis in Fig. 13) and the inlet water temperature in the condenser (legend of Fig. 13). Finally, Fig. 13 shows the variation of EER due to the partial load ratio. As can be noted in these graphs, the fits are acceptable. Therefore, these operating curves can be used to analyse air conditioning systems, just as recommended in the literature (Sánchez Ramos et al., 2019).

Figs. 14–15 show the generator temperature, condenser outlet temperature, and evaporator flow temperature estimated by the model on a randomly chosen pair of days. For this purpose, the flow rates and inlet temperatures of each of the loops are taken as data. The time step is 10 min, and each sample is referred to 1 h with a set of 6 data. The validation is performed during operating Mode 2 in the working regime.

On the other hand, Figs. 14–15 also show the estimates for each of the loops involved in the absorption machine: the condensation loop, heat input to the generator, and cold production in the evaporator. In addition to knowing the flow rates, the inlet water temperature (see green colour in Figs. 14–15) of each loop is taken as data. Based on these two temperatures, the response temperature of the case study can be estimated (see blue colour in Figs. 14–15) and measured (see red colour in Figs. 14–15). The generator temperature (upper graphs), the condensation water outlet temperature (middle graphs), and the discharge temperature of the cold to the building (lower graphs) can also be obtained. The model estimates respond to the trend of the measured values. Although the target results are not in a short time step (10 min), the model is run in this time step in order to be able to evaluate the operator decisions.

5. Results

This section shows the impact of chiller energy decision support on cooling production, minimising natural gas consumption and maximising the solar fraction. First, the importance of the chiller in the key performance indicators of the system is stressed. Second, the performance estimates of the entire solar cooling plant are validated. Third, the benefits of the application are justified.

5.1. Analysis of the initial situation

As mentioned previously, the absorption cooling system is provided with two possible heat inputs. The chiller receives heat from the solar field (priority) and the auxiliary gas boiler. During these years of experimentation (Bermejo et al., 2010), poor control over the system has been proven to generate a significant gas consumption. Therefore, this model has been developed to perform a predictive estimation of the chiller behaviour in order to minimise gas consumption. Fig. 16 shows the experimental results without (Fig. 16 up) using the energy manager for the chiller, which will further be compared with the results estimated with the decision support tool that optimises the system (Fig. 16 down).

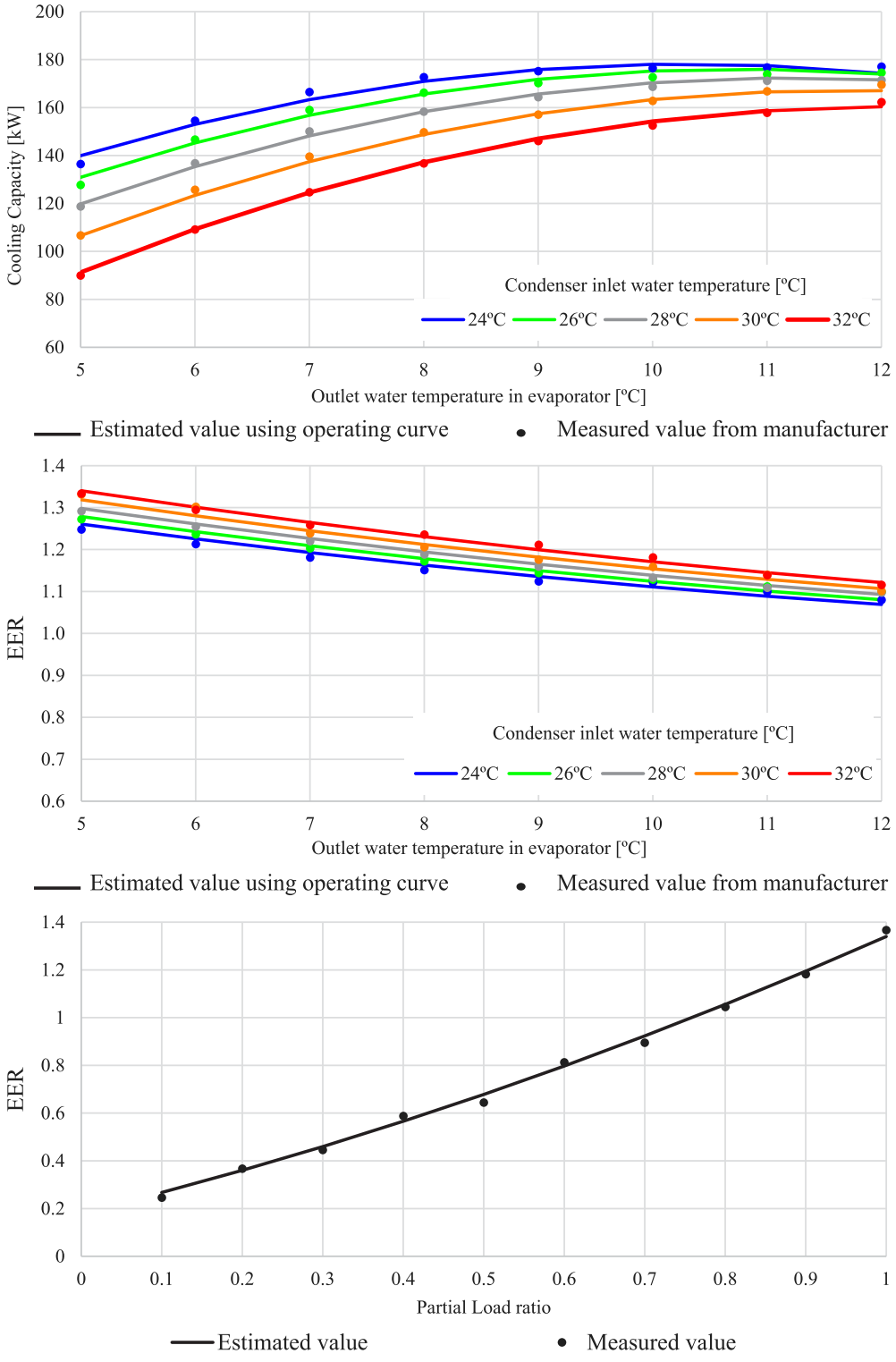

Fig. 13. Performance curves of the absorption chiller (provided by the manufacturer and implemented in the absorption chiller model).

On a typical sunny day, the average efficiency of the solar collector in the pilot solar plant is 0.35, with a maximum value of 0.40. When the collector water temperature rises 160 °C, a valve is opened so that the solar heating water reaches the generator and HTG heats up 145 °C. The operating mode prioritises the solar source upon the natural gas combustion. However, if the HTG drops below 145 °C after 30 min from start-up, the burner automatically switches on, providing a backup energy contribution to maintain the cooling power at approximately 135 kW. It should be noted that even so, most of the power supplied to

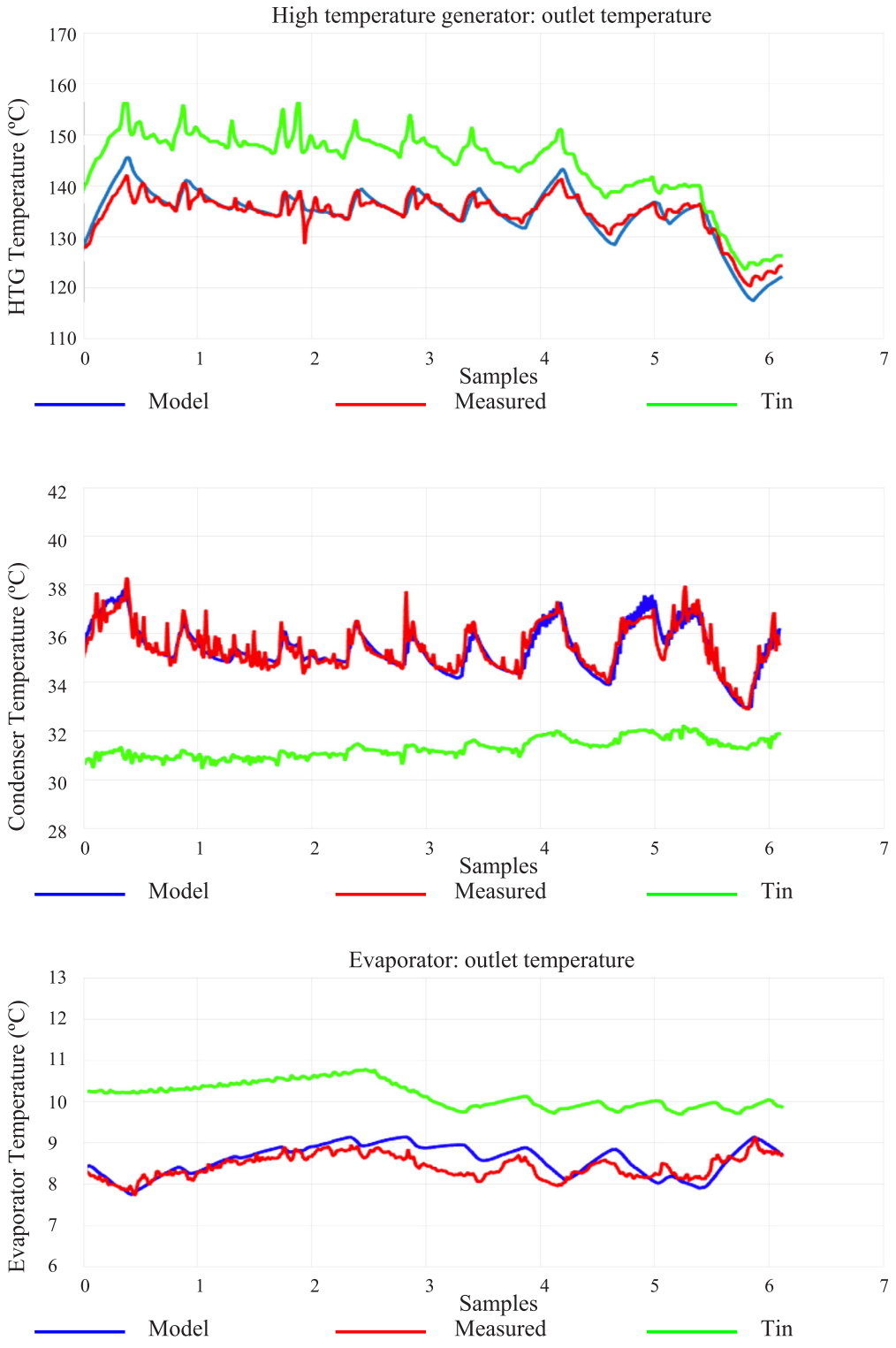

Fig. 14. First results of the model validation: Detailed results (Day 4). (For interpretation of the references to colour in this figure legend, the reader is referred to the web version of this article.)

the absorption chiller generator is provided by solar hot water (approximately 80%). Fig. 17 shows the evolution of the COP of the machine as the generator reaches this temperature. It is an interesting result because it allows knowing the real performance of the absorption chiller, being the maximum COP during the summer 1.45 and its average value 1.24.

Cooling needs of the building change along with cooling requirements throughout the day, with the highest levels corresponding to the 130–140 kW evaporator capacity. Similarly, the

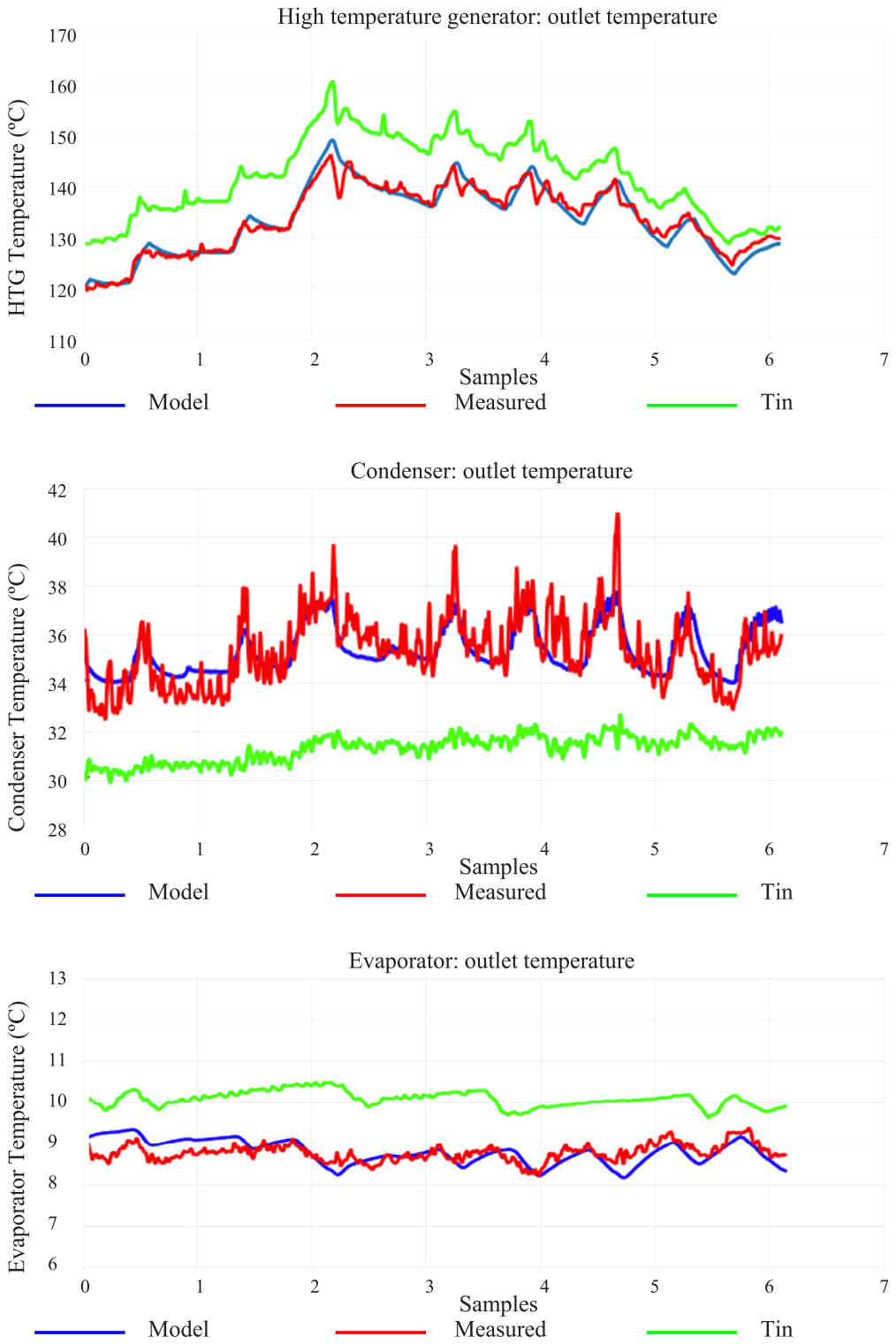

Fig. 15. First results of the model validation: Detailed results (Day 17). (For interpretation of the references to colour in this figure legend, the reader is referred to the web version of this article.)

COP also varies throughout the day. The initial two hours correspond to the transition period after start-up until the temperatures of the different chiller sections reach a stable status and the maximum COP value is achieved.

The Sankey diagram shown in Fig. 18 provides all the energy flows on a typical sunny day. Pipeline losses accounted for 20% of the total energy absorbed in the collector tubes. The absorption chiller COP was 1.16, and the SHF was 0.75, with the remaining 0.25 corresponding to the energy supplied by the natural gas for the HTG. In addition, the SCR reached 0.44.

The validation has been performed using 33 consecutive days of operation. The absorption machine model is running during these days, and its daily estimate is compared with the values measured. Representative daily measured data are summarised in Table A.1 in Appendix. It should be noted that the only reliable data are the operating flow rates and inlet temperatures of each

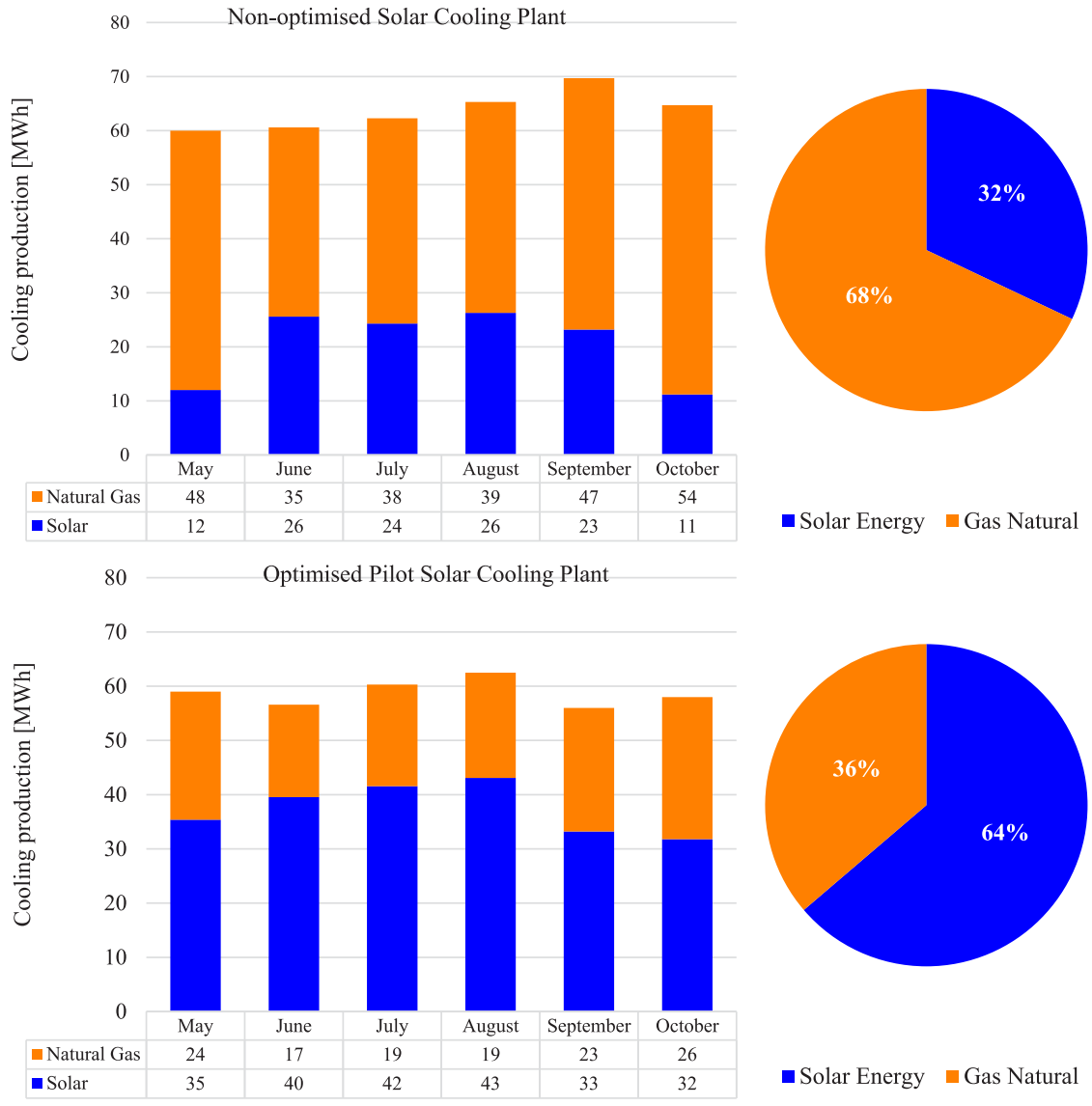

Fig. 16. Operation data of solar cooling plant during cooling season.

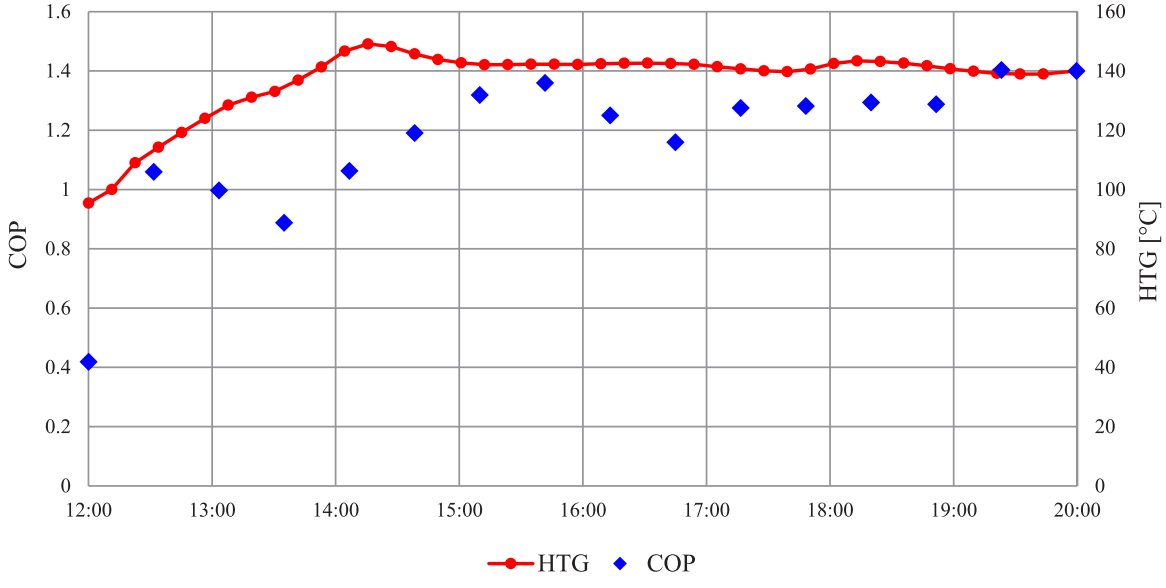

Fig. 17. Operation data of solar cooling plant during a typical day.

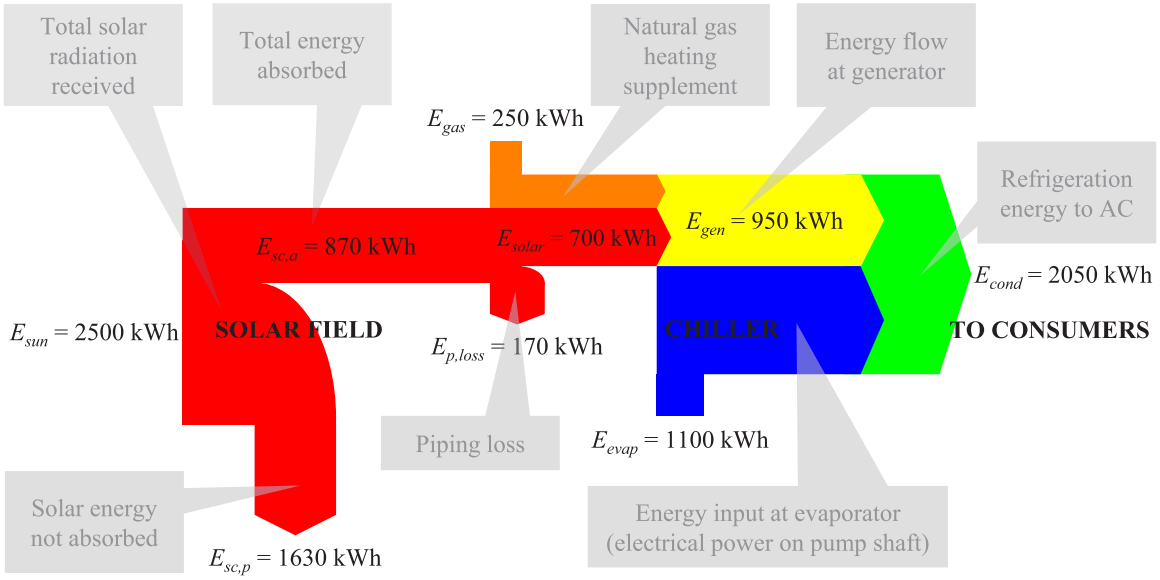

Fig. 18. Sankey diagram of a typical day validation of the plant operator.

Table 4
Results of validation of the solar cooling plant.

	Solar cooling plant			Solar cooling plant	
	Solar energy efficiency ratio –	Error %		Solar energy efficiency ratio –	Error %
Day 1	0.27	−0.1	Day 18	0.3	6
Day 2	0.26	1.6	Day 19	0.35	1.6
Day 3	0.29	−2.2	Day 20	0.33	5
Day 4	0.24	−3.3	Day 21	0.41	−2.5
Day 5	0.28	−3.2	Day 22	0.33	1.4
Day 6	0.23	4	Day 23	0.27	−3.4
Day 7	0.25	−2.2	Day 24	0.24	4
Day 8	0.24	−1.7	Day 25	0.16	−5.1
Day 9	0.25	0.3	Day 26	0.43	5.2
Day 10	0.39	−1.4	Day 27	0.37	−2.5
Day 11	0.38	−0.3	Day 28	0.36	2.7
Day 12	0.38	−6.1	Day 29	0.01	25.7
Day 13	0.18	−4.3	Day 30	0.28	−6.2
Day 14	0.27	0.4	Day 31	0.41	−0.6
Day 15	0.11	−0.4	Day 32	0.36	1.5
Day 16	0.36	5.3	Day 33	0.41	−2.8
Day 17	0.29	−2.5			

loop. These loops are the condensation circuit, evaporator cooling water, and solar plant generator.

Variables calculated are the thermal energy consumption of the solar installation, the natural gas consumption and the cooling energy production. Therefore, the main key performance indicators are the COP and the solar energy efficiency ratio. The COP is calculated as the quotient between the cooling energy produced and the thermal energy consumption of the absorption machine. In addition, the solar energy efficiency ratio is calculated as the quotient between the cooling production and the maximum solar energy captured in the primary receiver. Table A.2 in Appendix shows all the validation results. However, Table 4 and Fig. 19 summarise the most relevant results.

Relative errors obtained are low (which are shown in Table 4), proving the usefulness of the model for real-time predictive control or planning operating strategies for the system. In addition, the results are interesting because a plant efficiency higher than 40% is observed. The solar fraction of the solar cooling production system is more significant than 60% on average. It is a very useful result. The simplified methodology also fits nicely, being an easy and fast calculation solution.

5.2. Application of the inverse model for the plan operator

The inverse model is integrated into the management system of the plant as a predictive control tool. The model is executed using the actual data of the plant as its inputs. So, it estimates the behaviour of the chiller and decides the optimum partial load ratio of the auxiliary boiler to maximise the cooling production

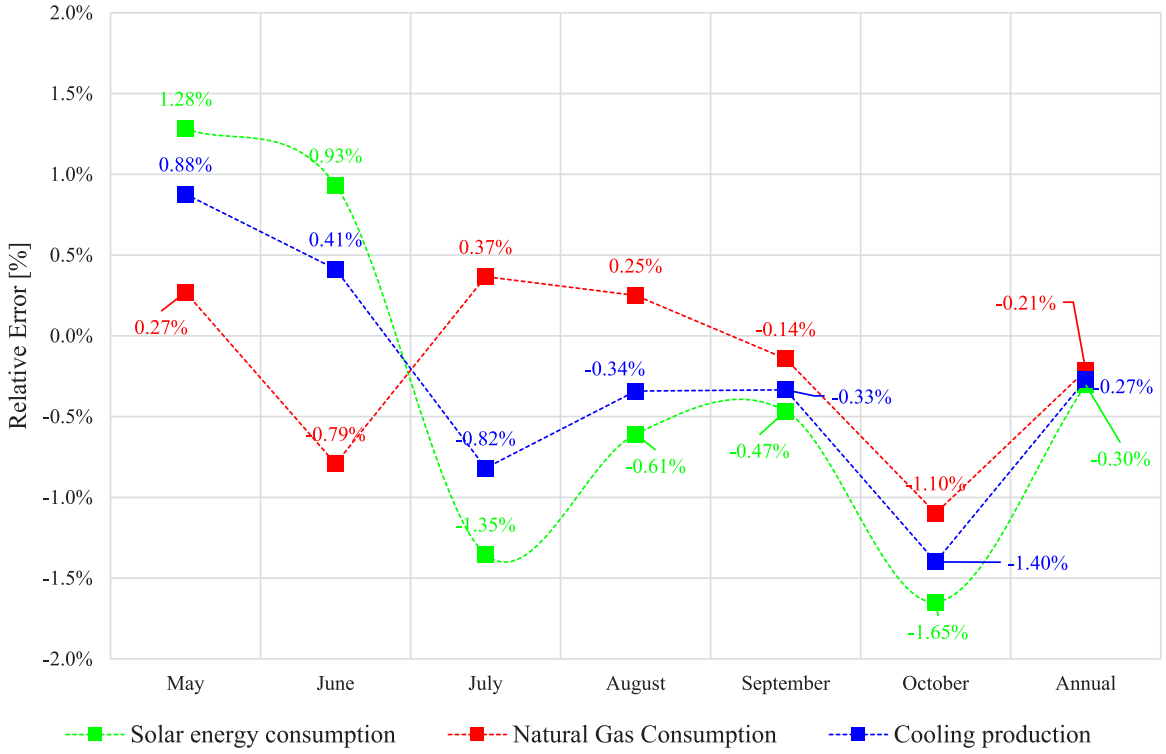

Fig. 19. Relative error of the model estimation (monthly and annual values).

Table 5
Operational costs with & without pilot plant and with & without predictive control.

Year	Scenario	Electricity consumption (MWh)	Natural gas consumption (MWh)	Cooling production (MWh)
1	Conventional system (measured)	171.41	0	720
2	Conventional system & pilot plant (measured)	108.72	264.59	822.79
2	Conventional system & pilot plant & predictive control (estimated)	106.91	134.52	822.79

and the solar fraction. So, it operates as a primary decision support system for the management system. The application allows validating how the proposed model improves the control of the plant by increasing the physical component of the system. Table 5 justifies the interest of this proposal, showing the measured consumption (MWh and €) of the building operation in three scenarios: without the pilot solar cooling plant (year 1), and with the solar cooling plant but without predictive control of the absorption system (year 2), as well as the estimation when the proposed model is implemented in the system management of the pilot solar cooling plant (year 2 too).

Table 5 shows the results of two different operation years. The first of them (year 1) does not include the solar cooling plant. The second one (year 2) integrates the solar cooling plant into the conventional system of the building. Regarding the results presented, although the conventional chiller achieves a very high COP (higher than 4, as shown in Table 5, year 1), the improvement of the whole system thanks to the pilot plant can be checked. However, despite this improvement, it is still possible to save an additional 49% of the natural gas consumption and 16% of the total cost if the absorption chiller operates optimally (third scenario). This is thanks to the predictive control of the auxiliary boiler to heat the generator when hot water from the Fresnel solar collector varies.

6. Conclusions

In this research, an absorption chiller has been coupled with the energy management model of a solar cooling plant by means of an inverse model. The model is connected to the manufacturer data and the experimental data by identifying its parameters. This allows the replicability of the model for other chillers or conditions, as demonstrated by the validation performed. Furthermore, the usability of this model is validated by its integration into the control system of the plant. Therefore, the paper eliminates the performance gaps and solves the integration with the renewable source.

The research also shows an experimental analysis to optimise an absorption chiller. With these experimental data, it has been possible to know the real operation of this system. In addition, a characterisation model is proposed, whose parameters use readily available experimental data. This model predicts the behaviour of the system in the case of changes in the input energy flows or in the control system. The model is robust, as demonstrated by the validation performed, whose experiments have been shown to be

Table A.1
Representative daily measured data.

Measured data		Solar Fresnel Collector			Absorption Chiller					Solar cooling plant
		Incident Solar Energy	Absorbed Solar Energy	Thermal energy storage	Solar Heat Supplied	Gas Heat Supplied	Cooling Production	COP	Solar Fraction	Solar energy efficiency ratio
	Data	kWh	kWh	kWh	kWh	kWh	kWh	-	-	-
Day 1	25-5	2595	734	161	555	75	806	1.28	0.88	0.27
Day 2	26-5	2677	719	200	597	117	843	1.18	0.84	0.26
Day 3	27-5	2607	725	205	580	73	836	1.28	0.89	0.29
Day 4	7-6	2362	768	306	536	30	577	1.02	0.95	0.23
Day 5	8-6	2233	692	199	547	55	662	1.10	0.91	0.27
Day 6	9-6	2121	606	244	428	21	530	1.18	0.95	0.24
Day 7	10-6	2428	702	153	531	48	637	1.10	0.92	0.24
Day 8	14-6	2282	667	122	533	165	705	1.01	0.76	0.23
Day 9	15-6	2305	628	188	540	120	713	1.08	0.82	0.25
Day 10	21-6	2583	924	114	798	266	1309	1.23	0.75	0.38
Day 11	22-6	2622	938	116	816	251	1302	1.22	0.76	0.38
Day 12	23-6	2489	761	135	704	615	1688	1.28	0.53	0.36
Day 13	24-6	1887	491	165	320	755	1097	1.02	0.3	0.17
Day 14	27-6	2605	815	138	823	712	1305	0.85	0.54	0.27
Day 15	28-6	2040	424	167	261	360	553	0.89	0.42	0.11
Day 16	2-8	2481	926	136	886	579	1568	1.07	0.6	0.38
Day 17	9-8	2278	672	111	655	695	1310	0.97	0.49	0.28
Day 18	10-8	2279	764	113	743	644	1332	0.96	0.54	0.32
Day 19	12-8	2386	800	115	767	546	1444	1.10	0.58	0.35
Day 20	13-8	2408	836	-14	788	602	1473	1.06	0.57	0.35
Day 21	14-8	2366	826	83	829	660	1683	1.13	0.56	0.40
Day 22	15-8	2340	806	30	798	543	1287	0.96	0.6	0.33
Day 23	29-8	2133	595	107	534	373	934	1.03	0.59	0.26
Day 24	31-8	2016	528	46	486	655	1187	1.04	0.43	0.25
Day 25	1-9	1674	408	106	286	462	666	0.89	0.38	0.15
Day 26	20-9	1604	546	82	540	582	1526	1.36	0.48	0.46
Day 27	21-9	1928	618	23	585	796	1671	1.21	0.42	0.36
Day 28	22-9	1864	605	-5	554	315	1069	1.23	0.64	0.37
Day 29	23-9	1195	253	261	12	723	904	1.23	0.02	0.02
Day 30	26-9	1782	490	18	436	763	1319	1.10	0.36	0.27
Day 31	12-10	1750	643	28	607	308	1071	1.17	0.66	0.40
Day 32	13-10	1566	552	45	555	777	1372	1.03	0.42	0.37
Day 33	14-10	1517	522	37	527	319	964	1.14	0.62	0.39

very accurate, easy to reproduce, and adaptable to any absorption chiller system. Moreover, the results prove that:

- To model the behaviour of this technology in three sections is interesting in order to be able to adjust the dynamics of the system. The three stages are start-up, regular operation and shutdown. The detailed validation results indicate a good approximation of the estimates made with acceptable errors.
- The application performed shows that the coupling of the model in higher-order energy simulation tools may be interesting. Because of the daily and seasonal estimates of renewable consumption, yields or fractions match those obtained in the experiments. This evidences that it is still

Table A.2
Results of validation: Absorption chiller.

	Absorption Chiller									
	Estimated Solar Heat Consumption	Error	Estimated Gas Heat Consumption	Error	Estimated Cooling Production	Error	Estimated COP	Error	Estimated Solar Fraction	Error
	kWh	%	kWh	%	kWh	%	-	%	-	%
Day 1	554	0.1	74	1.6	805	0.1	1.28	-0.2	0.88	-0.4
Day 2	602	-0.9	121	-3.0	836	0.8	1.16	2.0	0.83	1.7
Day 3	586	-1.1	71	2.9	853	-2.0	1.30	-1.4	0.88	0.8
Day 4	548	-2.2	30	0.7	597	-3.4	1.03	-1.4	0.93	2.3
Day 5	542	0.9	55	0.5	685	-3.4	1.15	-4.3	0.92	-0.7
Day 6	418	2.2	21	1.7	507	4.3	1.15	2.2	0.97	-2.6
Day 7	546	-2.8	47	2.1	650	-2.1	1.10	0.3	0.90	2.6
Day 8	519	2.6	170	-3.3	724	-2.7	1.05	-3.9	0.77	-1.7
Day 9	538	0.4	119	1.2	711	0.3	1.08	-0.3	0.82	-0.3
Day 10	798	0.0	264	0.9	1324	-1.1	1.25	-1.3	0.75	-0.2
Day 11	807	1.1	254	-1.3	1305	-0.3	1.23	-0.7	0.77	-1.1
Day 12	718	-2.0	590	4.0	1730	-2.5	1.32	-3.3	0.54	-1.5
Day 13	329	-2.9	719	4.8	1092	0.4	1.04	-2.2	0.31	-1.8
Day 14	833	-1.2	657	7.7	1255	3.8	0.84	0.9	0.55	-2.3
Day 15	266	-2.1	337	6.3	528	4.4	0.87	1.7	0.43	-2.9
Day 16	887	-0.1	602	-3.9	1494	4.7	1.00	6.2	0.60	0.8
Day 17	651	0.6	704	-1.3	1369	-4.5	1.01	-4.1	0.48	1.4
Day 18	758	-2.0	651	-1.1	1256	5.6	0.82	6.1	0.53	2.3
Day 19	773	-0.8	542	0.8	1403	2.9	1.07	3.0	0.58	-0.6
Day 20	796	-1.0	618	-2.7	1417	3.8	1.00	5.4	0.56	2.2
Day 21	830	-0.1	650	1.5	1722	-2.3	1.16	-3.0	0.56	0.0
Day 22	806	-1.0	529	2.6	1262	2.0	0.95	1.5	0.60	0.4
Day 23	542	-1.5	356	4.6	944	-1.1	1.05	-2.1	0.59	-0.8
Day 24	500	-2.8	691	-5.4	1167	1.6	0.98	5.7	0.41	5.0
Day 25	294	-2.9	455	1.4	677	-1.7	0.90	-1.5	0.38	-0.4
Day 26	525	2.8	608	-4.5	1499	1.8	1.32	2.7	0.48	0.7
Day 27	595	-1.8	822	-3.3	1712	-2.5	1.21	0.2	0.41	1.8
Day 28	560	-1.0	285	9.6	1005	6.0	1.19	3.3	0.66	-2.5
Day 29	12	1.8	760	-5.1	879	2.7	1.14	7.4	0.02	22.2
Day 30	443	-1.7	701	8.1	1302	1.3	1.14	-3.4	0.38	-5.8
Day 31	604	0.4	310	-0.8	1076	-0.5	1.18	-0.5	0.66	-0.5
Day 32	539	2.9	707	9.0	1312	4.4	1.05	-2.2	0.45	-6.1
Day 33	530	-0.6	316	0.9	981	-1.8	1.16	-1.7	0.62	-0.4

possible to save almost 50% of natural gas consumption with the same cooling production.

Finally, the proposed procedure for characterising an absorption chiller and providing a solution for modelling this type of technology may be used as a methodology for evaluating and diagnosing these units. If these systems are in real operation, the values obtained by monitoring them can be compared with the estimates made with the curves proposed under the same conditions. This model can also be integrated into real-time predictive control for solar cooling facilities. This inverse model would allow solving the definition of optimal operating strategies. The results prove the interest of the model. Furthermore, the proposed methodology can be applied to any hybrid solar system for whatever control requirements.

CRediT authorship contribution statement

MCarmen Guerrero Delgado: Methodology, Investigation, Formal analysis, Writing – original draft. **Jose Sánchez Ramos:** Software, Validation, Data curation, Investigation, Conceptualization. **Daniel Castro Medina:** Experimental facility, Investigation. **Teresa Rocío Palomo Amores:** Simulation, Investigation, Visualization. **Alberto Cerezo-Narváez:** Conceptualization, Writing, Resources. **Servando Álvarez Domínguez:** Conceptualisation, Methodology, Supervision, Formal analysis.

Declaration of competing interest

The authors declare that they have no known competing financial interests or personal relationships that could have appeared to influence the work reported in this paper.

Acknowledgements

The European Commission funded this study under the project MedEcoSuRe - "Mediterranean University as Catalyst for Eco-Sustainable Renovation" (A_B.4.3_0218) to eliminate Fresnel Solar's barriers Cooling Plants as a potential energy-efficient alternative in university buildings. Also, this study has been co-financed by the European Regional Development Funds (ERDF).

Appendix

See Tables A.1 and A.2.

References

Ahn, H., Rim, D., Pavlak, G.S., Freihaut, J.D., 2019. Uncertainty analysis of energy and economic performances of hybrid solar photovoltaic and combined cooling, heating, and power (CCHP + PV) systems using a Monte-Carlo method. Appl. Energy 255, 113753. http://dx.doi.org/10.1016/j.apenergy.2019.113753.

Ali, D., Ratismith, W., 2021. A semicircular trough solar collector for air-conditioning system using a single effect NH3–H2O absorption chiller. Energy 215, 119073. http://dx.doi.org/10.1016/j.energy.2020.119073.

Amiri Rad, E., Davoodi, V., 2021. Thermo-economic evaluation of a hybrid solar-gas driven and air-cooled absorption chiller integrated with hot water production by a transient modeling. Renew. Energy 163, 1253–1264. http://dx.doi.org/10.1016/j.renene.2020.08.157.

Anon, 2018. DOE2.com home page. http://www.doe2.com/. (Accessed 28 December 2018).

Anon, 2021. Third party certification | Certita Eurovent. https://www.eurovent-certification.com/es. (Accessed 19 February 2021).

Araújo, A., Silva, R., 2020. Energy modeling of solar water heating systems with on-off control and thermally stratified storage using a fast computation algorithm. Renew. Energy 150, 891–906. http://dx.doi.org/10.1016/j.renene.2020.01.026.

Bataineh, K., Taamneh, Y., 2016. Review and recent improvements of solar sorption cooling systems. Energy Build. 128, 22–37. http://dx.doi.org/10.1016/j.enbuild.2016.06.075.

Bermejo, P., Pino, F.J., Rosa, F., 2010. Solar absorption cooling plant in Seville. Sol. Energy 84, 1503–1512. http://dx.doi.org/10.1016/j.solener.2010.05.012.

Bilardo, M., Ferrara, M., Fabrizio, E., 2020. Performance assessment and optimization of a solar cooling system to satisfy Renewable Energy Ratio (RER) requirements in multi-family buildings. Renew. Energy http://dx.doi.org/10.1016/j.renene.2020.03.044.

Castro, J., Farnós, J., Papakokkinos, G., Zheng, J., Oliet, C., 2020. Transient model for the development of an air-cooled LiBr-H2O absorption chiller based on heat and mass transfer empirical correlations. Int. J. Refrig. 120, 406–419. http://dx.doi.org/10.1016/j.ijrefrig.2020.08.030.

Chen, J.F., Dai, Y.J., Wang, R.Z., 2017. Experimental and analytical study on an air-cooled single effect LiBr-H2O absorption chiller driven by evacuated glass tube solar collector for cooling application in residential buildings. Sol. Energy 151, 110–118. http://dx.doi.org/10.1016/j.solener.2017.05.029.

Chen, Y., Wang, J., Lund, P.D., 2020. Sustainability evaluation and sensitivity analysis of district heating systems coupled to geothermal and solar resources. Energy Convers. Manag. 220, 113084. http://dx.doi.org/10.1016/j.enconman.2020.113084.

DOE, 2010. EnergyPlus - Engineering reference.

European Commission, 2018. Directive (EU) U) 2018/844. Off. J. Eur. Union 2018, 75–91.

Evola, G., Le Pierrès, N., Boudehenn, F., Papillon, P., 2013. Proposal and validation of a model for the dynamic simulation of a solar-assisted single-stage LiBr/water absorption chiller. Int. J. Refrig. 36, 1015–1028. http://dx.doi.org/10.1016/j.ijrefrig.2012.10.013.

Florides, G.A., Kalogirou, S.A., Tassou, S.A., Wrobel, L.C., 2002. Modelling, simulation and warming impact assessment of a domestic-size absorption solar cooling system. Appl. Therm. Eng. 22, 1313–1325. http://dx.doi.org/10.1016/S1359-4311(02)00054-6.

Gallego, A.J., Sánchez, A.J., Berenguel, M., Camacho, E.F., 2020. Adaptive UKF-based model predictive control of a Fresnel collector field. J. Process Control 85, 76–90. http://dx.doi.org/10.1016/j.jprocont.2019.09.003.

Ibrahim, N.I., Khan, M.M.A., Mahbubul, I.M., Saidur, R., Al-Sulaiman, F.A., 2017. Experimental testing of the performance of a solar absorption cooling system assisted with ice-storage for an office space. Energy Convers. Manag. 148, 1399–1408. http://dx.doi.org/10.1016/j.enconman.2017.07.001.

International Energy Agency, 2013. Transition to sustainable buildings: Strategies and opportunities to 2050. http://dx.doi.org/10.1787/9789264202955-en.

Jalalizadeh, M., Fayaz, R., Delfani, S., Mosleh, H.J., Karami, M., 2021. Dynamic simulation of a trigeneration system using an absorption cooling system and building integrated photovoltaic thermal solar collectors. J. Build. Eng. 43, 102482. http://dx.doi.org/10.1016/j.jobe.2021.102482.

Jradi, M., Riffat, S., 2014. Tri-generation systems: Energy policies, prime movers, cooling technologies, configurations and operation strategies. Renew. Sustain. Energy Rev. 32, 396–415. http://dx.doi.org/10.1016/j.rser.2014.01.039.

Karki, S., Haapala, K.R., Fronk, B.M., 2019. Investigation of the combined efficiency of a solar/gas hybrid water heating system. Appl. Therm. Eng. 149, 1035–1043. http://dx.doi.org/10.1016/j.applthermaleng.2018.12.086.

Klein, S.A., 2010. TRNSYS 17: A Transient System Simulation Program. vol. 1, Sol. Energy Lab. Univ. Wisconsin, Madison, USA, pp. 1–5.

Kylili, A., Fokaides, P.A., 2015. European smart cities: The role of zero energy buildings. Sustain. Cities Soc. 15, 86–95. http://dx.doi.org/10.1016/j.scs.2014.12.003.

Leckner, M., Zmeureanu, R., 2011. Life cycle cost and energy analysis of a Net Zero Energy House with solar combisystem. Appl. Energy 88, 232–241. http://dx.doi.org/10.1016/j.apenergy.2010.07.031.

Lubis, A., Jeong, J., Giannetti, N., Yamaguchi, S., Saito, K., Yabase, H., Alhamid, M.I., Nasruddin, 2018. Operation performance enhancement of single-double-effect absorption chiller. Appl. Energy 219, 299–311. http://dx.doi.org/10.1016/j.apenergy.2018.03.046.

Mao, M., Cui, L., Zhang, Q., Guo, K., Zhou, L., Huang, H., 2020. Classification and summarization of solar photovoltaic MPPT techniques: A review based on traditional and intelligent control strategies. Energy Rep. 6, 1312–1327. http://dx.doi.org/10.1016/j.egyr.2020.05.013.

Martínez, J.C., Martinez, P.J., Bujedo, L.A., 2016. Development and experimental validation of a simulation model to reproduce the performance of a 17.6 kW LiBr–water absorption chiller. Renew. Energy 86, 473–482. http://dx.doi.org/10.1016/j.renene.2015.08.049.

Nikbakhti, R., Wang, X., Hussein, A.K., Iranmanesh, A., 2020. Absorption cooling systems – Review of various techniques for energy performance enhancement. Alex. Eng. J. 59, 707–738. http://dx.doi.org/10.1016/j.aej.2020.01.036.

Prieto, A., Knaack, U., Auer, T., Klein, T., 2019. COOLFACADE: State-of-the-art review and evaluation of solar cooling technologies on their potential for façade integration. Renew. Sustain. Energy Rev. 101, 395–414. http://dx.doi.org/10.1016/j.rser.2018.11.015.

Ray, M., Samal, P., Panigrahi, C.K., 2021. The influencing factors on efficacy enhancement of HVAC systems – A review. Mater. Today Proc. http://dx.doi.org/10.1016/j.matpr.2021.07.264.

Rivarolo, M., Greco, A., Massardo, A.F., 2013. Thermo-economic optimization of the impact of renewable generators on poly-generation smart-grids including hot thermal storage. Energy Convers. Manag. 65, 75–83. http://dx.doi.org/10.1016/j.enconman.2012.09.005.

Sánchez Ramos, J., Delgado, Mc.C. Guerrero, Álvarez Domínguez, S., Molina Félix, J.L., Cabeza, L.F., 2019. Gas engine heat pump system: Experimental facility and thermal evaluation for 5 different units. Energy Convers. Manag. 199, 112060. http://dx.doi.org/10.1016/j.enconman.2019.112060.

Santamouris, M., Adnot, J., Álvarez Domínguez, S., Klitsikas, N., Orphelin, M., Lopes, C., Sánchez de la Flor, F.J., 2004. Cooling the cities - Raifraichir les villes. Ecole des Mines de Paris. Les Presses, Paris.

Sarabia Escriva, E.J., Lamas Sivila, E.V., Soto Frances, V.M., 2011. Air conditioning production by a single effect absorption cooling machine directly coupled to a solar collector field. Application to Spanish climates. Sol. Energy 85, 2108–2121. http://dx.doi.org/10.1016/j.solener.2011.05.019.

Sebastián, A., Abbas, R., Valdés, M., Rovira, A., 2021. Modular micro-trigeneration system for a novel rotatory solar Fresnel collector: A design space analysis. Energy Convers. Manag. 227, 113599. http://dx.doi.org/10.1016/j.enconman.2020.113599.

Settino, J., Sant, T., Micallef, C., Farrugia, M., Spiteri Staines, C., Licari, J., Micallef, A., 2018. Overview of solar technologies for electricity, heating and cooling production. Renew. Sustain. Energy Rev. 90, 892–909. http://dx.doi.org/10.1016/j.rser.2018.03.112.

Sharafi, M., ElMekkawy, T.Y., Bibeau, E.L., 2015. Optimal design of hybrid renewable energy systems in buildings with low to high renewable energy ratio. Renew. Energy 83, 1026–1042. http://dx.doi.org/10.1016/j.renene.2015.05.022.

Shirazi, A., Taylor, R.A., Morrison, G.L., White, S.D., 2018. Solar-powered absorption chillers: A comprehensive and critical review. Energy Convers. Manag. 171, 59–81. http://dx.doi.org/10.1016/j.enconman.2018.05.091.

Song, Z., Ji, J., Cai, J., Li, Z., Gao, Y., 2020. Performance prediction on a novel solar assisted heat pump with hybrid Fresnel PV plus TEG evaporator. Energy Convers. Manag. 210, 112651. http://dx.doi.org/10.1016/j.enconman.2020.112651.

Wang, J., Li, X., Wang, B., Wu, W., Song, P., Shi, W., 2017. Performance comparison between an absorption-compression hybrid refrigeration system and a double-effect absorption refrigeration sys-tem. Procedia Eng. 205, 241–247. http://dx.doi.org/10.1016/j.proeng.2017.09.959.

Xu, Z.Y., Wang, R.Z., 2017. Comparison of CPC driven solar absorption cooling systems with single, double and variable effect absorption chillers. Sol. Energy 158, 511–519. http://dx.doi.org/10.1016/j.solener.2017.10.014.

Yu, J., Li, Z., Chen, E., Xu, Y., Chen, H., Wang, L., 2019. Experimental assessment of solar absorption-subcooled compression hybrid cooling system. Sol. Energy 185, 245–254. http://dx.doi.org/10.1016/j.solener.2019.04.055.

Zhao, T., Chen, X., Chen, Q., 2020. Heat current method-based modeling and optimization of the single effect lithium bromide absorption chiller. Appl. Therm. Eng. 175, 115345. http://dx.doi.org/10.1016/j.applthermaleng.2020.115345.